Structure

Article

Antibody-like recognition of a γδ T cell receptor toward a foreign antigen

Graphical abstract

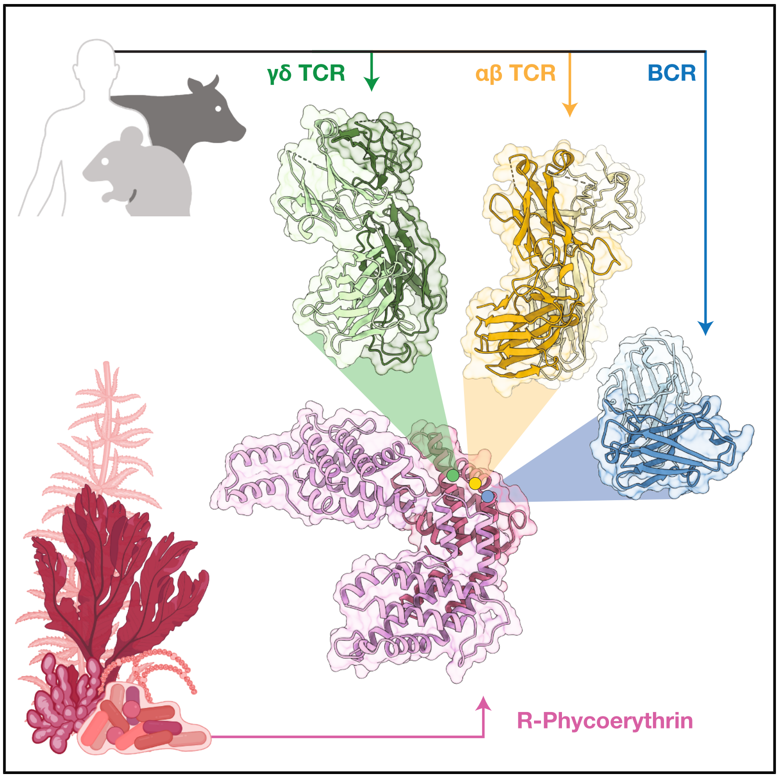

Authors

Liam Rashleigh,
Hariprasad Venugopal,
Michael T. Rice, ..., Dale I. Godfrey,
Jamie Rossjohn, Benjamin S. Gully

Correspondence

jamie.rossjohn@monash.edu (J.R.),
ben.gully@monash.edu (B.S.G.)

In brief

Rashleigh et al. utilized phycoerythrin, a bacterial derived protein, to explore immune reactivity of B cells, αβ T cells, and γδ T cells. All lymphocytes directly recognized PE, while T cell recognition resulted in cellular activation. Structural characterization revealed a shared manner of recognition by distinct receptor lineages.

Highlights

- γδTCRs, αβTCR, and antibody fragment bind directly to PE
- TCR recognition of PE induces proximal signaling and cellular activation
- Cryo-EM structures of γδTCR, αβTCR, and antibody fragment bound to PE
- Convergent recognition mode of all three lymphocyte receptor lineages

Rashleigh et al., 2025, Structure *33*, 1–14
October 2, 2025
https://doi.org/10.1016/j.str.2025.07.006

CellPress

Please cite this article in press as: Rashleigh et al., Antibody-like recognition of a γδ T cell receptor toward a foreign antigen, Structure (2025), https://doi.org/10.1016/j.str.2025.07.006

Structure

CellPress
OPEN ACCESS

Article

Antibody-like recognition of a γδ T cell receptor toward a foreign antigen

Liam Rashleigh,[1] Hariprasad Venugopal,[1] Michael T. Rice,[1] Sachith D. Gunasinghe,[1,5] Chhon Ling Sok,[1] Nicholas A. Gherardin,[2] Catarina F. Almeida,[2] Ildiko Van Rhijn,[3] D. Branch Moody,[3] Dale I. Godfrey,[2] Jamie Rossjohn,[1,4,6,7,*] and Benjamin S. Gully[1,5,6,*]

[1]Infection and Immunity Program & Department of Biochemistry and Molecular Biology, Biomedicine Discovery Institute, Monash University, Clayton, VIC, Australia

[2]Department of Microbiology & Immunology, Peter Doherty Institute for Infection and Immunity, University of Melbourne, Melbourne, VIC, Australia

[3]Division of Rheumatology, Inflammation, and Immunity, Brigham and Women's Hospital and Harvard Medical School, Boston, MA, USA

[4]Institute of Infection and Immunity, Cardiff University, School of Medicine, Cardiff, UK

[5]Present address: Olivia Newton-John Cancer Research Institute and School of Cancer Medicine, La Trobe University, Heidelberg, VIC 3084, Australia

[6]Senior author

[7]Lead contact

*Correspondence: jamie.rossjohn@monash.edu (J.R.), ben.gully@monash.edu (B.S.G.)

https://doi.org/10.1016/j.str.2025.07.006

SUMMARY

The antigen recognition principles of B cells and αβ T cells have been well described compared to those of the γδ T cell. By way of their specificity conferring receptor (γδTCR), γδ T cells can directly bind proteinaceous antigens. A known γδ T cell and B cell model antigen is phycoerythrin (PE), a light harvesting protein from rhodophytes and cyanobacteria. Here we probed human γδTCR reactivity to PE, in which a Vδ1Vγ5 TCR bound directly to induce proximal signaling and cellular activation. We determined the cryoelectron microscopy (cryo-EM) structure of the γδTCR-phycoerythrin immune complex. We then determined the cryo-EM structures of an antibody fragment and an αβTCR bound to PE. This revealed convergent use of apical aromatic residues to mediate contacts with a common PE epitope. Comparative analyses of the γδTCR revealed multiple antibody-like characteristics, including an enrichment of apical aromatic residues. Our findings reveal further distinct facets of antigen recognition by the γδTCR.

INTRODUCTION

The adaptive immune system consists of highly specific lymphocyte lineages including αβ T cells, B cells, and γδ T cells.[1] γδ T cells exhibit features associated with both adaptive and innate immunity, including possessing T cell antigen receptors (TCRs) and having the potential for rapid effector functions.[2] γδ T cells have associations with anti-viral, anti-bacterial, wound repair, and anti-tumor immunity, yet the ligands triggering these functional responses remain largely unknown.[3–5] αβTCRs typically recognize peptides, lipids and small molecule metabolites presented by major histocompatibility complex (MHC),[6] CD1, or MR1 molecules, respectively.[7] In contrast, B cells directly recognize antigens that are neither processed nor presented. These differing recognition strategies are achieved by receptors uniquely expressed by that lymphocyte lineage, despite having similar immunoglobulin-based architectures. The antigen recognition principles of γδ T cells are comparatively less well understood but are thought to have vestiges of both antibodies and αβTCRs. Presently it remains unclear how the γδTCR endows γδ T cells with antibody-like poly-specificity.[8] Although our understanding of γδ T cell ligands is incomplete,[9] their antigen repertoire includes multiple MHC class-I-like molecules,[10–15] as well as the structurally distinct butyrophilin (BTN) and butyrophilin-like molecules.[16–20] In recognizing these ligands, γδ T cells are thought to operate as homeostatic sentinels, recognizing host stress or aberrance.[21] Structures of γδTCR-antigen complexes have indicated antibody-like recognition mechanisms and such variable antigen engagement angles are permitted by the remarkable flexibility of its membrane-bound receptor complex.[22–24]

A notable feature of γδ T cells is their γδTCR-mediated reactivity to ligands outside of the BTN/MHC-like axis, including ephrin type A receptor 2, aminoacyl tRNA synthetase, annexin A2, phycoerythrin[16] (PE), and small molecule conjugates such as cyanine 3-ovalbumin.[8,25–29] Precisely how γδ T cells recognize such a broad spectrum of antigens remains unknown. Moreover, the rhodophyte (red algae) photosystem protein, r-phycoerythrin, presents as an obscure antigen, with recurrent observations of B cell and γδ T cell reactivity observed as well as a recent report of an αβTCR recognizing PE.[28,30–32]

Here, we determine the cryoelectron microscopy (cryo-EM) structure of a γδTCR bound to a model non-self-antigen, PE.

CellPress OPEN ACCESS

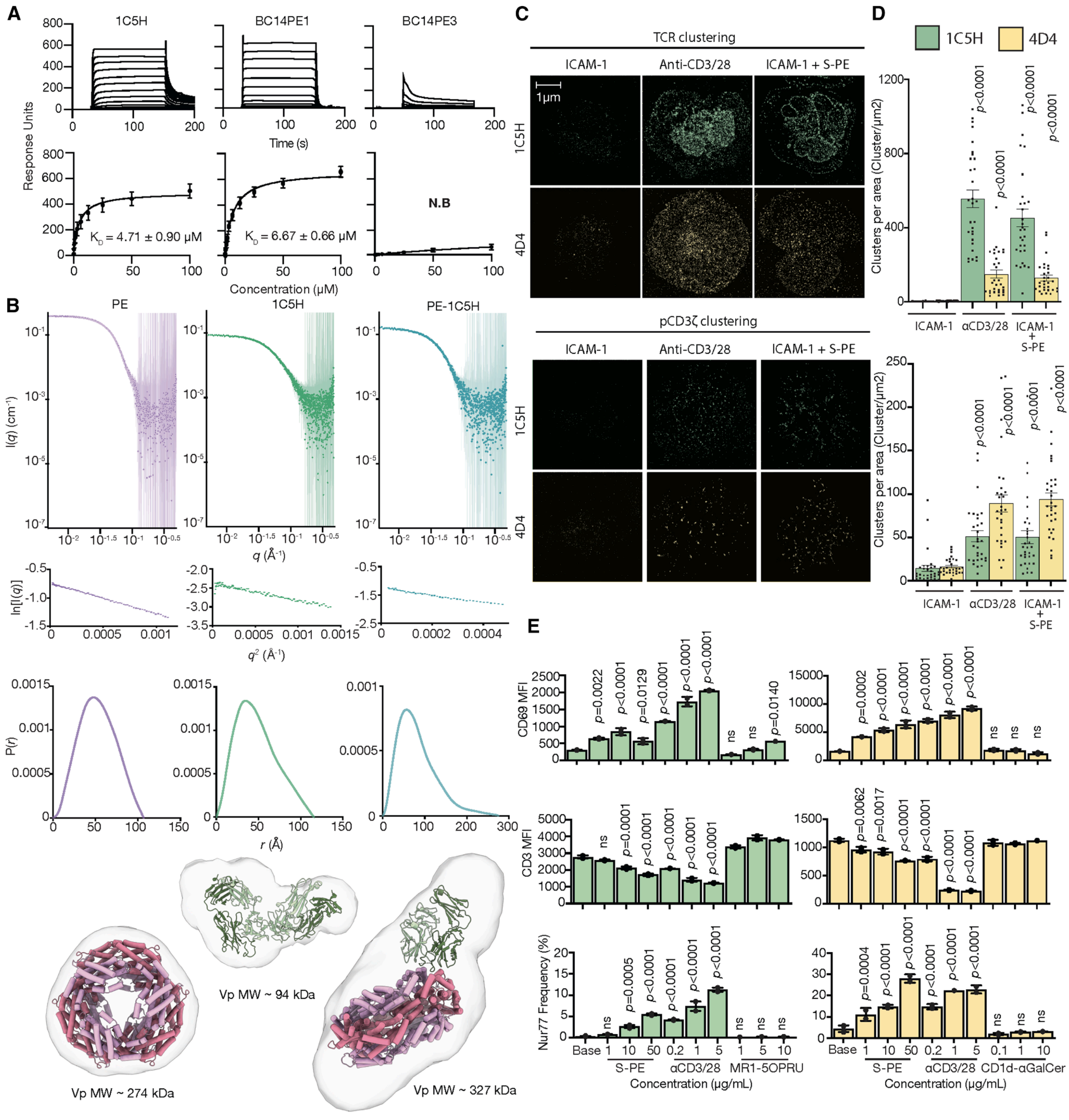

Figure 1. TCRs confer reactivity to PE conducive of lymphocyte activation

(A) SPR steady-state affinity measurements of TCR-PE interactions shown as representative sensorgrams (top) and equilibrium binding curves (bottom). Two independent experiments each comprising two repeat measurements were used to estimate the dissociation constants (K_D). Error bars represent mean and standard error of the mean (SEM) from two experiments. N.B, no binding.

(B) Small angle X-ray scattering curves, Guinier plots, P(r) distribution plots and averaged *ab initio* reconstructions for PE, 1C5H γδTCR, and the 1C5H-PE complex. Molecular weights (MWs) were estimated from the Porod volume (Vp), displayed for each profile.

(C) Representative single-molecule images depicting TCR clustering in Jurkat cells expressing 1C5H and BW58 cells expressing 4D4. Cells were stimulated on supported lipid bilayers decorated with ICAM-1 (unstimulated control) or anti-CD3/CD28, or ICAM-1 with the S-PE (scale bars, 1 μm). Single-molecule images showing the clustering of phosphorylated CD3ζ (pCD3ζ) in the same TCR-transduced cells under the same stimulation conditions. TCRs on cells were stained with a primary antibody targeting the human CD3ε (Jurkat) or mouse TCRβ subunit (BW58), conjugated to Alexa Fluor 647.

(D) Quantification of TCR and pCD3ζ clustering was performed using DBSCAN analysis with varying cluster parameters. The analysis reflects ≥30 measurements from two independent experiments, each consisting of $n \geq 15$ cells. Error bars represent the SEM.

(legend continued on next page)

Our structure provides insight into γδTCR reactivity to an intact protein antigen and reveals mechanisms where a distended CDR3δ used key aromatic contacts to bind to PE. We also determined the cryo-EM structure of a single-chain variable fragment (scFv) region of an antibody in complex with PE, and a cryo-EM structure of the 4D4 αβTCR-PE complex, previously determined via X-ray crystallography.[31] This enabled a broader comparison of how immunoreceptors from three lymphocyte lineages recognize a common antigen. Analysis of antigen receptor structure and sequence revealed antibody-like characteristics in the recognition of diverse ligands by γδTCRs. These include the tertiary structure, as well as the composition and structure of the δ-chain IgV domain.

RESULTS

γδTCRs binding to an intact foreign antigen

To understand how γδTCRs directly recognize foreign protein antigens, we focused on PE, a known model antigen of B cells, peripheral γδ T cells, and a murine αβ T cell.[28,31,33] Specifically, we examined PE-reactive human γδTCRs that were identified alongside our previous study of the PE-reactive murine αβTCR clone 4D4.[31] We first produced soluble versions of the $V\delta1^+V\gamma5^+$ (termed 1C5H), $V\delta1^+V\gamma3^+$ (termed BC14PE1), and $V\delta3^+V\gamma4^+$ (termed BC14PE3) γδTCRs (Figure S1). To directly measure PE-reactivity and specificity, we conducted affinity measurement analyses using surface plasmon resonance (SPR) with immobilized PE. Neither the 1C5H nor the BC14PE1 γδTCRs bound to the negative control, human MR1-5-OP-RU, whereas the MR1-reactive αβTCR, AF7, did not bind PE but bound MR1, dissociation constant (K_D) = 2.18 ± 0.19 μM (Figure S2).[34] The 1C5H and BC14PE1 γδTCRs bound immobilized PE, K_D = 4.71 ± 0.90 and K_D = 6.67 ± 0.66 μM, respectively, within a typical range for γδTCR-antigen interactions[9] (Figure 1A). However, BC14PE3 showed no detectable PE binding in these experiments, which may reflect PE isoform specificity as noted previously.[28,31] The mouse PE-reactive αβTCR, 4D4, also bound PE with comparable affinity, K_D = 6.54 ± 0.41 μM, as previously shown (Figure S2).[31] The 1C5H γδTCR was selected for further investigation due to its high affinity, specificity, and slow dissociation rate for PE recognition. To gain insight into how the 1C5H γδTCR bound to PE, we utilized size exclusion chromatography coupled with small angle X-ray scattering (SEC-SAXS). The resultant SEC-SAXS data of the 1C5H γδTCR and PE samples revealed radially averaged scattering profiles, forward scattering and *ab initio* reconstruction consistent with a homogeneous particle of the size and shape of a soluble γδTCR "dimer-of dimers" and PE hetero-hexamer, which we will refer to as a PE oligomer (Figures 1B and S3). The 1C5H γδTCR dimer replicates recent observations wherein the Vγ5 domain mediates γδTCR dimerization to form a Vγ5-Vγ5 interface, in which ablation of dimer formation arrested receptor activation.[23,24] SAXS analyses of the 1C5H γδTCR-PE sample clearly indicated complex formation in solution with the *ab initio* reconstruction revealing a 1C5H γδTCR bound to the PE oligomer (Figures 1B and S3). These results revealed the capacity of soluble PE-reactive γδTCRs to form specific complexes with intact PE in solution.

γδTCR reactivity toward an intact foreign antigen

To confirm signaling competency, we used Jurkat T cells, lacking endogenous TCR, expressing the 1C5H γδTCR alongside 4D4 αβTCR-transduced BW58 cells that served as a control (Figure S4). We used single molecule imaging to probe the initial triggering events of cellular activation, namely TCR-clustering and proximal signaling via CD3ζ phosphorylation. Cell line controls 2C12 and G83.C4 displayed increased TCR clustering and receptor phosphorylation upon antigen exposure to CD1d-α-GalCer and MR1-5-OP-RU, respectively. (Figure S4). Imaging of cells interacting with ICAM-1-bearing supported lipid bilayers functionalized with streptavidin-PE (S-PE) showed a significant ($p < 0.001$) increase in the amount of 1C5H TCR clusters relative to ICAM-1 alone (Figures 1C and 1D). TCR-cluster size and density were unaffected (Figure S4) despite antigen stimulation potently inducing receptor phosphorylation (Figures 1C and 1D). The 4D4 cell line showed increased TCR clustering and receptor phosphorylation upon S-PE exposure (Figures 1C and 1D). The 1C5H TCR showed atypical evidence of TCR-pre-clustering (Figure S4), potentially due to its dimerization capacity as indicated in SAXS analyses. The γδTCR can require a larger amount of antigen for comparable levels of CD3ζ phosphorylation.[22] Utilizing the same TCR-transduced cell lines, we assessed the capacity of PE reactive clones to produce distal markers of T cell activation and performed activation assays using titrating amounts of plate bound S-PE, anti-CD3 stimulating monoclonal antibody as well as either human MR1-5-OP-RU or murine CD1d-α-GalCer controls. The murine CD1d-α-GalCer reactive αβTCR 2C12[35] and human MR1-5-OP-RU reactive γδTCR G83.C4[14] were included as controls, producing dose-dependent CD69 and Nur77 upregulation in response to their cognate ligands: mouse CD1d-α-GalCer and human MR1-5-OP-RU, respectively (Figure S4), but not in response to PE stimuli. Conversely, 4D4 or 1C5H did not show signs of activation to plate bound mouse CD1d-α-GalCer or human MR1-5-OP-RU controls (Figure 1E). S-PE stimulation resulted in specific and dose-dependent upregulation of the downstream signaling markers CD69 and Nur77, and downregulation of CD3 in both the 1C5H and 4D4 cell lines (Figure 1E) but not the control cell lines (Figure S4), indicative of PE antigen-specific signaling. Thus, PE-recognition by the 1C5H γδTCR can drive proximal signaling to induce cellular activation.

The cryo-EM structure of a γδTCR-PE complex

To elucidate the molecular basis for this reactivity, we next imaged the 1C5H γδTCR-PE complex by cryo-EM to yield a

(E) Mean fluorescence intensity (MFI) of CD69 expression (top), or CD3 expression (middle) among 4D4 and 1C5H TCR-transduced cells at 16 h after incubation with S-PE, murine CD1d-α-GalCer, or human MR1-5-OP-RU at titrated concentrations (0.1–10 nM). Frequency of Nur77-expressing 4D4 and 1C5H TCR-transduced cells was also assessed after 2 h (bottom).

Data represent two experimental repeats of duplicate titrations shown as dots (average of duplicate), error bars represent the SEM. *p* values represent significance from baseline. Statistical significance was determined using one-way analysis of variance (ANOVA) followed by Tukey's multiple comparisons test (D and E).

Please cite this article in press as: Rashleigh et al., Antibody-like recognition of a γδ T cell receptor toward a foreign antigen, Structure (2025), https://doi.org/10.1016/j.str.2025.07.006

Table 1. Structural refinement and validation statistics

Model	1C5H-PE	4D4-PE	CL33-PE	PE alone	1C5H dimer
PDB ID	PDB: 9O62	PDB: 9MKO	PDB: 9MGB	PDB: 9O61	PDB: 9O60
EMDB ID	EMD: 70157 (composite) EMD: 70139 (consensus)	EMD: 48332	EMD: 48248	EMD: 70156	EMD: 70155 (TCR local refinement)
Chains	20	20	24	18	3
Nonhydrogen atoms	19,381	19,575	26,862	16,392	3,634
Protein residues	2,425	2,460	3,390	2,040	449
Ligands	PUB: 6 PEB: 24	PUB: 6 PEB: 24	PUB: 6 PEB: 24	PUB: 6 PEB: 24	– –
Bonds (RMSD)					
Length	0.005	0.007	0.005	0.005	0.005
Angles	0.967	1.002	0.618	0.950	0.658
MolProbity score	1.79	1.42	1.8	1.60	2.3
Clash score	13.78	7.63	10.22	12.37	19
Ramachandran plot (%)					
Outliers	0.34	0.04	0.03	0.35	0.23
Allowed	2.44	1.61	2.87	1.29	8.24
Favored	97.23	98.35	97.1	98.36	91.53
Rotamer outliers (%)	0.99	2.06	1.38	0.94	3
Model vs. data					
CC (mask)	0.83	0.86	0.85	0.91	0.69
CC (box)	0.67	0.83	0.86	0.83	0.53
CC (peaks)	0.65	0.79	0.82	0.81	0.34
CC (volume)	0.82	0.86	0.86	0.91	0.70
Mean CC for ligands	0.79	0.76	0.76	0.82	–

consensus reconstruction at gold standard Fourier shell correlation 0.143 of 2.03 Å (Figure S5). Additional focused refinements of the 1C5H γδTCR and PE reached global resolutions (GSFSC = 0.143) of 2.63 Å and 1.70 Å, respectively, the latter approaching the Nyquist limit. In concert, the consensus and focused reconstructions yielded high-resolution features across most of the protein complex, particularly the 1C5H γδTCR-PE interface, which enabled reliable model building, refinement, and validation (Table 1). Overall, the 1C5H γδTCR-PE reconstruction revealed a single 1C5H γδTCR bound to the PE oligomer, with clear density showing that the interaction was mediated via the complementarity determining regions (CDRs) of the γδTCR (Figure 2A). We first used the high-resolution focused reconstruction of the PE oligomer to aid in model building for each of the six PEαβ heterodimers and refined their alpha helical globin-like domains. The 1C5H γδTCR bound to a single PE heterodimer within the context of the PE hetero-hexameric oligomer. Here, the 1C5H γδTCR δ-chain, orchestrated PE recognition, in that it comprised ∼68% of the total buried surface area (BSA) of 1,840 Å^2, comparable to other γδTCR complexes (Figures 2B and S6).[12,14,15,36] The δ-chain dominance at the PE interface was largely attributable to the CDR3δ loop that composed over half of the interface (52.6% BSA) although all the CDR loops contributed to varying extents (CDR1δ 10%, CDR2δ 5.6%, CDR1γ 16.5%, CDR2γ 1.1%, and CDR3γ 14.2% BSA) (Figure 2B). The 1C5H γδTCR CDR3δ loop is elongated due to the inclusion of extensive N-region additions flanking the *TRDD3*01* element to result in a 38 amino acid CDR3δ (from TRDV*01 to the TRDJ3*01). Molecular recognition of PE by the 1C5H γδTCR relied upon contacts from each of these elements, including a prominent role the *TRDD3*01*-encoded W100δ that protruded from the CDR3δ loop to bind between the B- and E-helices of the PE α-chain (Figure 2C). Here the W100δ hydrogen bonded to D87α of the PE chain E-helix and was stabilized by extensive van der Waals (vdW) contacts between W100δ and the PE surface, primarily Y83α (Figure 2C). The preceding Y99δ stabilized K81α and E77α with a hydrogen bond to each (Figure 2C). Together, W100δ and Y99δ contacted N80α of PE via dual backbone hydrogen bonds, with N80α also interacting with S31δ within the CDR1δ (Figure 2D). In turn, S31δ also contacted Q76α of the PE E-helix with hydrogen bonds to the carboxyl backbone of Y32δ and E55δ of the CDR2δ loop also stabilizing the PE Q76α sidechain. The Vδ region was enriched with ancillary aromatic residues providing further vdW contacts, inclusive of W109δ (Figure 2C), W30δ and Y33δ (Figure 2D). W100δ was indeed the largest contributor to this interface, closely followed by the neighboring Y99δ that occupied a cleft between the PEα and β-chains. (Figure 2C). The neighboring non-germline-encoded H97δ of the CDR3δ loop formed an intra-TCR hydrogen bond to the carboxyl backbone of R100 γ of the CDR3γ loop, which in turn made a salt bridge contact with E77α of the E-helix N-terminus (Figure 2E). Other 1C5H γ-chain interactions with the PE β-chain occurred via CDR1γ-mediated vdW contacts, namely by N29γ and F31γ

Please cite this article in press as: Rashleigh et al., Antibody-like recognition of a γδ T cell receptor toward a foreign antigen, Structure (2025), https://doi.org/10.1016/j.str.2025.07.006

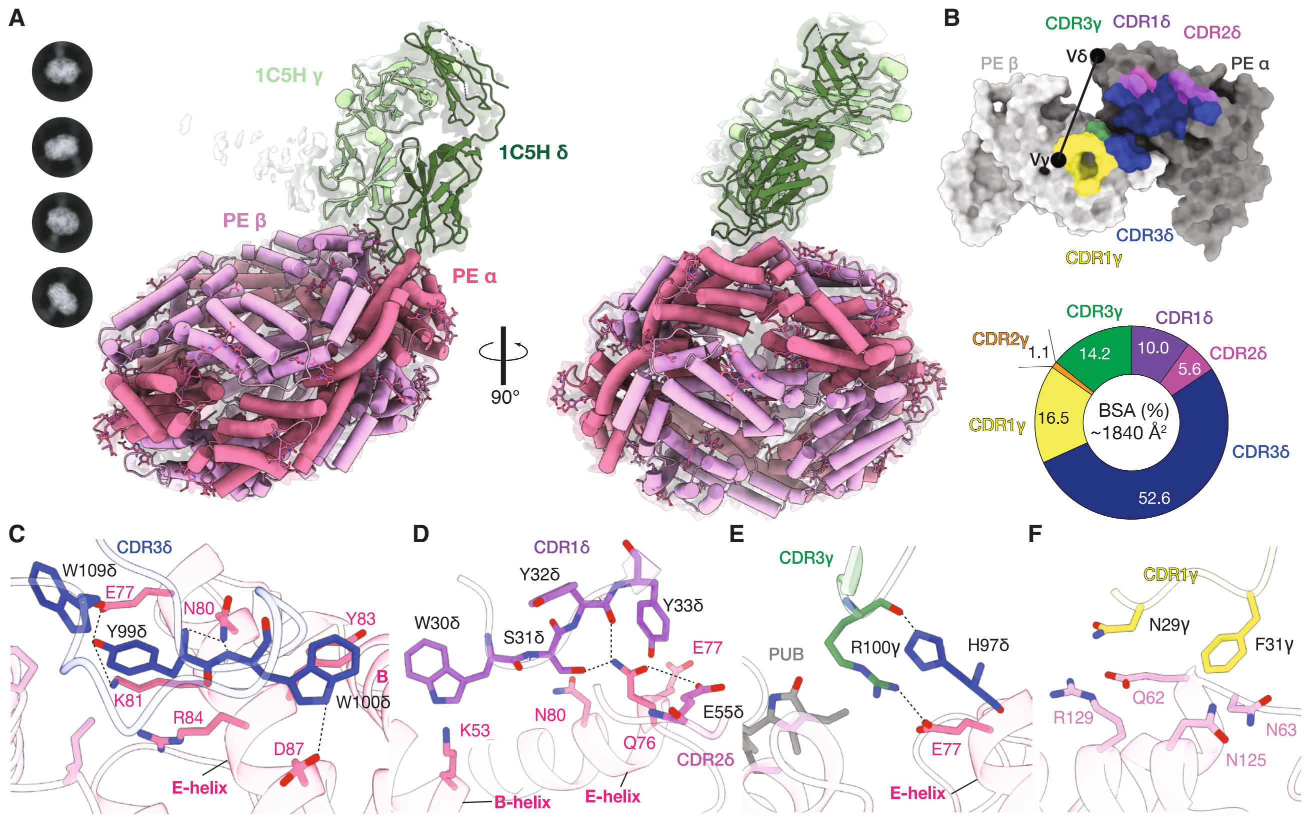

Figure 2. Structural basis of 1C5H γδTCR recognition of PE

(A–F) (A) The 1.91 Å cryo-EM (composite) map of 1C5H (in green) bound to PE (in pink) overlayed with the resultant structure of the 1C5H-PE immune complex. Accompanied by representative 2D classification images. (B) Surface map of PE recognition interface with contact-regions colored according to CDR-mediated recognition with percentage contribution of each CDR to total BSA as shown in the circular graph below. Balls on top show centers of mass of Variable γ or variable δ chains of TCR over the PE surface. (C) CDR3δ-mediated interactions with PE. (D) CDR1δ-mediated interactions with PE. (E) CDR3γ-mediated interactions with PE. (F) CDR1γ-mediated interactions with PE.

For (C–E), interacting residues are shown as sticks. 1C5H residues are labeled in black, PE α-peptide residues are labeled in pink, and PE β-peptide residues are labeled in light pink. Hydrogen bond and salt bridge interactions are shown as black dashed lines. Not all contact residues are displayed. PUB, phycourobilin.

(Figure 2F). The 1C5H γδTCR-PE cryo-EM structure revealed the molecular basis of direct antigen reactivity, thereby revealing a prominent role for an elongated CDR3δ and apical aromatic residues.

A γδTCR dimer

Focused refinements enabled additional structural characterization of individual components of the observed immune complex. The previously mentioned 1.70 Å focused refinement of unbound PE (Figure 3A) enabled high-resolution model building of the of *Porphyra tenera* light harvesting complex (Figures 3B–3D). The 2.63 Å focused refinement of the 1C5H γδTCR revealed density corresponding to a second γδTCR, bound alongside the Vγ domain (Figure 3E). This corroborated the SAXS evidence of the 1C5H γδTCR dimerization in solution and single molecule imaging suggesting 1C5H γδTCR-pre-clusters prior to antigen binding (Figures S3 and S4). 1C5H γδTCR dimerization was mediated via a ∼1,160 $Å^2$ BSA Vγ5-Vγ5 interface, meaning that the CDR loops of the second 1C5H TCR were unbound by PE. Each 1C5H TCR would not occlude the other symmetrical PE epitopes. However, obligate 1C5H dimerization would preclude other TCR dimers from occupying these epitopes. Although clear density for the entire second 1C5H γδTCR was evident, sidechains were only placed for the Vγ5 domain (Figure 3F), the complete secondary 1C5H γδTCR can be modeled from this chain placement (Figure 3G). The Vγ5-Vγ5 dimerization interface comprised the symmetrical D- and E-strand contacts, including Y69γ and the flanking H71γ of the D-strand that formed stacking and hydrogen bonds with Y69γ′ and E20γ′ of the second Vγ5 (termed Vγ5′), respectively (Figure 3H). The neighboring E-strand R83γ completed the interface with hydrogen contacts to the D57γ′ sidechain and S55γ′ backbone of the CDR2γ, of the Vγ5′. These interactions corroborated observations of Vγ5-Vγ5 dimerization within $Vγ5^+Vδ1^+$ crystal structures, and cryo-EM structures of the $Vγ5^+Vδ1^+$ TCR-CD3 integral membrane complex[12,23,24] (Figures 3I and 3J). Thus, this observation shows that dimerization appears to be common across γδTCRs encoding the $Vγ5^+$ domain and may prove to be an obligate dimer.

The cryo-EM structures of an antibody fragment and an αβTCR bound to PE

PE has been previously described as a B cell antigen, and used as a crucial tool to study the formation of memory B cells.[33,37] In Igh^b mice, up to 90% of the PE-specific memory B cell clones

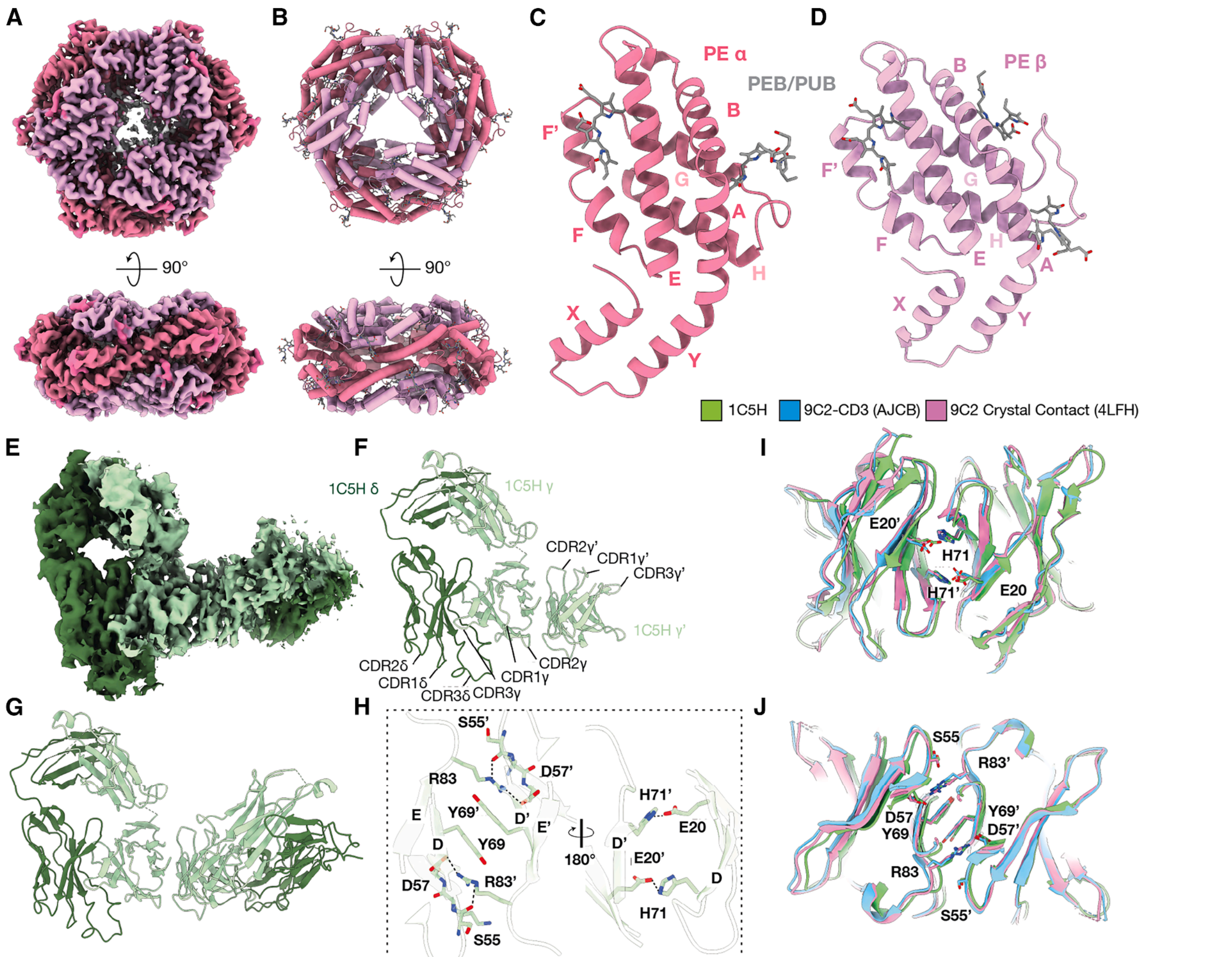

Figure 3. Cryo-EM structures of unbound PE and 1C5H γδTCR dimer

(A) The 1.7 Å cryo-EM map of unbound PE.

(B–D) (B) Subsequent refined structural model of the hetero-hexameric PE oligomer. (C) Single subunit of the PEα peptide. (D) Single subunit of the PEβ peptide. Each subunit's architectural helix is labeled; phycoerythrobilins (PEB) and phycourobilins (PUB) are shown in gray.

(E) TCR focused refinement revealing a map with secondary 1C5H γδTCR (excluding PE density).

(F) Resultant modeled coordinates of the 1C5H γδTCR bound to secondary 1C5H Vγ domain.

(G) The stacking interactions driving Vγ5 dimerization.

(H) Modeled dimer arrangement of complete secondary 1C5H TCR.

(I and J) Overlay comparison of Vγ5 dimer interface displaying stacking interactions of 1C5H, 9C2 (cryo-EM, 8JCB) and 9C2 (crystal contact, 4LFH) dimerization.

expressed an *Ighv1-81* gene segment and naive B cell responses were ablated by blocking with a monoclonal antibody Fab fragment (CL33).[30] We produced a scFv of the CL33 antibody (Figure S1) and examined PE binding using SPR. The CL33 scFv bound PE with an affinity (K_D) of 10.20 ± 0.84 nM (Figure 4A), in keeping with antibody-ligand interactions being of higher affinity than TCR-ligand interactions.[7,38] Early structural characterization via negative stain electron microscopy of the CL33-PE complex revealed 2D classes consistent with at least three CL33 scFvs bound to a PE oligomer although preferred orientations limited further analyses (Figures 4B and S3). We then determined the scFv CL33-PE complex using cryo-EM to a global resolution of 2.30 Å (Figure S7; Table 1). The structure revealed six CL33 scFv fragments bound to the PE hetero-hexamer (Figure 4C), with the higher receptor occupancy likely stemming from the increased affinity of the CL33 fragment. The CL33 scFv bound an overlapping epitope of the PE α-chain to the 1C5H TCR, the 1,780 Å^2 (BSA) interface was dominated by the IgHV, as is common for these genes, which comprised ∼65% of the interface via the CDR2H and CDR3H, replicating the CDR3δ dominance of the 1C5H TCR (Figure 4D).[39]

As is common in antibody-ligand interactions, the CL33 scFv paratope for PE-binding comprised several aromatic residues including neighboring tyrosines.[40] Firstly, the CDR3H Y106H and Y107H doublet bound the same hydrophobic pocket of the A, B, and E helices of the α-peptide as the 1C5H-γδTCR, whereby the latter occupied the pocket and formed a hydrogen bond with D87α and the former stacks atop contacting E49α (Figure 4E). CDR3H-mediated contact continued with a hydrogen bond between N108H and Q76α as well as considerable vdW interactions provided by residues mentioned and notable others including S109H, A107H, K53α, N80α, and Y83α (Figure 4E).

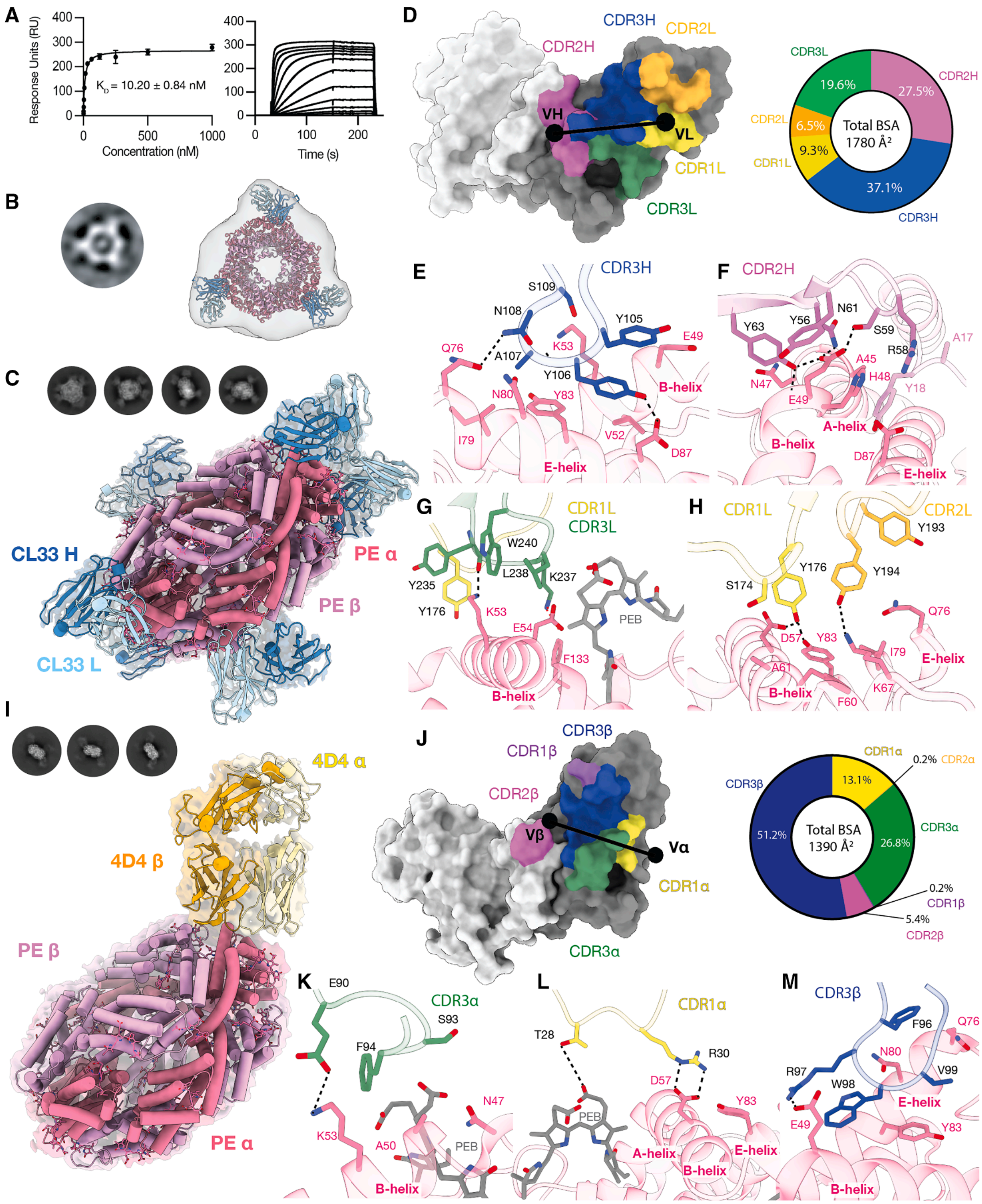

Figure 4. Structural basis of CL33 scFv and 4D4 αβTCR recognition of PE

(A) SPR binding affinity measurements of CL33-PE binding as affinity curves (left) and representative sensorgrams (right) of CL33 over immobilized PE. Two independent experiments each comprising two repeat measurements were used to estimate the dissociation constant (K_D). Error bars represent mean and SEM from two experiments. N.B, no binding. K_D measured from two independent expressions of analyte in duplicate.

(B) Negative stain electron microscopy reconstruction of CL33 bound to PE with an inset 2D class average from a similar orientation.

(C) The 2.3 Å cryo-EM map of CL33-bound PE overlayed with the resultant structure of the CL33-PE immune complex. Accompanied by a representative 2D class average from a similar orientation.

(D and E) (D) Surface of PE recognition interface, contacts colored according to CDR-mediated recognition. Spheres represent centers of mass of the variable regions. Percentage contribution of each chain and each CDR to total BSA (E) CDR3H-mediated interactions with PE.

(F–H) (F) CDR2H-mediated interactions with PE, (G) CDR1L/CDR3L-mediated interactions with PE, and (H) CDR1L/CDR2L-mediated interactions with PE.

(I) The 3.4 Å cryo-EM map of 4D4-bound PE overlayed with the resultant structure of the 4D4-PE immune complex. Accompanied by representative 2D classification images.

(legend continued on next page)

E49α was further capped by two tyrosines of the CDR2H, Y56H, and Y63H, which formed vdW contacts and electrostatic interactions between A and B helices of the PE α-chain, the latter forming hydrogen bonds to both the backbone and sidechain of E49α (Figure 4F). CDR2H-mediated E49α contacts continued through hydrogen bonds with N61H and S59H, stabilizing the receptor-ligand complex (Figure 4F). CDR3L contact residues are highlighted by a salt bridge formation through K237L and E54α (Figure 4G) as well as the backbone of Y235L forming a hydrogen bond to K53α. Similar to E49α in Figure 3F, K53α is capped by aromatic sidechains namely Y235L, W240L, and Y176L (Figure 4G). CDR1L and CDR2L employed a triad of tyrosines to contact the PE α-chain; Y176L of the CDR1L makes hydrogen contacts to both D57α and Y83α, while Y194L of CDR2L forms a hydrogen bond with K67α (Figure 4H). Thus, the scFv bound to a common epitope on the PE surface as the 1C5H TCR, both largely mediated via apical CDR3 aromatic residues.

We next determined the 4D4 αβTCR-PE complex via cryo-EM to complete the structural comparisons of adaptive immunoglobulin receptors against a common antigen using the same technique. The 4D4 TCR-bound PE was resolved to a resolution of 3.4 Å (Figures 4I and S8; Table 1). The cryo-EM structure mirrored the recently determined X-ray crystal structure of the 4D4 αβTCR-PE complex.[31] The lower occupancy of TCRs per PE hetero-hexamer likely stems from a lower sample concentration during cryo-EM, compared to crystallography. The 4D4 interface with PE principally involved the CDR3β loop, which contributed to more than half of the total 1,390 $Å^2$ BSA (Figure 4J). The molecular drivers of 4D4 αβTCR recognition of PE included key residues of the CDR3β (51.2% total BSA), followed by CDR3α (26.8%) and CDR1α (13.1%) (Figure 4J). K53 of the PE α-chain forms a hydrogen bond to the sidechain of E90α within the CDR3α, with F94α mediating further backbone interactions with A50 and N47 sidechains of the PE α-chain (Figure 4K). CDR1α contacts are mediated by a dual salt bridge formation of R30α to D57 of the PE α-chain, and further interaction with Y83 of PE α-chain, while T28α contacts a phycoerythrobilin (PEB) ligand (Figure 4L). W98β of the CDR3β occupied the same epitope on the PE surface as W100δ of the 1C5H γδTCR and Y106H of the CL33 scFv, namely a pocket formed by the A, B, and E helices of the PE α-chain (Figure 4M). This positioning was further stabilized by other residues within the CDR3β, namely R97β salt bridge formation with E49 of the PE α-chain. The 4D4 αβTCR recognizes the same PE epitope as CL33 scFv and 1C5H γδTCR, utilizing a notably reduced amount of aromatic residue contacts while sustaining PE reactivity.

γδ T cells utilize antibody-like characteristics during recognition of a conserved PE epitope

Overall cryo-EM analysis of 1C5H γδTCR, CL33 scFv, and 4D4 αβTCR reveals similarities between PE recognition of three different receptors of lymphoid origin. Despite varied docking modes and recognition footprints, all three receptor interfaces converged upon the PE α-chain (Figure 5A), namely a hydrophobic pocket comprising the A, B, and E helices of the α-peptide (Figure 5A). Each of the three receptors utilized an apical aromatic residue within the CDR3 loop to occupy this cleft, W100δ of the 1C5H γδTCR, Y106H of the CL33 scFv heavy chain and W98β of the 4D4 αβTCR (Figure 5B). These residues each contributed the largest BSA contribution of any residue within the respective receptor interfaces. We next performed site-directed mutagenesis of the γδTCR and scFv CDR3 aromatic residues to measure their impact on receptor binding via SPR. Mutation of the 1C5H CDR3δ apical aromatic residues Y99Aδ and W100Aδ ablated PE-reactivity normalized to wild type, whereas the F31A mutation of the CDR1γ loop had a minimal impact on binding (~4-fold K_D increase from wild-type control) (Figures 1A, 5C, and S2). Conversely, despite binding within the same pocket within the scFv-PE complex, the Y106A mutation of the CL33 CDR3H did not ablate PE-reactivity. The Y106A mutation did largely impact PE binding affinity (~18-fold K_D increase), however less so than the Y63A mutation in the H-chain which reduced the CL33 scFv affinity to 1.43 ± 0.12 μM (~116-fold K_D increase) (Figures 5C and S2). Overall, despite the involvement of apical CDR aromatic residues in scFv and γδTCR recognition of PE, the γδTCR was reliant upon a few key aromatic residues whereas the scFv had less reliance on each aromatic residue, potentially a redundancy resulting from affinity maturation in antibodies.

Broadly, the total BSA was greatest in γδTCR recognition of PE (1,840 $Å^2$), closely followed by scFv recognition (1,780 $Å^2$), while the BSA for the αβTCR-PE complex was distinctly smaller at 1,390 $Å^2$. Regarding shape complementarity (Sc) at the interfaces, γδTCR and scFv recognition of PE share similarities with scores of 0.69 and 0.70, respectively, while the Sc at the αβTCR-PE interface was only 0.50 (Figure 5D). Comparing the number of aromatic residues at the interface showed that the γδTCR and scFv utilized an increased number of aromatics at the interface (Figure 5E). In these aspects, 1C5H γδTCR recognition of PE is more aligned with CL33 antibody recognition of PE than 4D4 αβTCR recognition. A sequence independent structure-based search, centered on the PE α-chain recognized by the immune receptors, identified homology to the globin-like superfamily. Analysis of the most homologous structures revealed explicit conservation of a ligand-binding pocket (Figures 5F and 5G). Thus, the PE epitope that is commonly recognized by the 1C5H γδTCR, CL33 scFv, and the 4D4 αβTCR is highly conserved across the globin-like superfamily.

Antibody-like mechanisms underpin γδTCR-ligand interactions

To more broadly understand the molecular drivers of antibody-like recognition by the γδTCR, we turned to the expanding γδTCR-MHC-like antigen literature.[12–15,41,42] Within the context of MHC-like structures, we aimed to further define the distinguishing features of γδTCR-antigen recognition, relative to antibodies and αβTCRs. Comparisons of the structures revealed that the γδTCR bound diverse structural epitopes across the

(J–M) (J) Surface of PE recognition interface, contacts colored according to CDR-mediated recognition and percentage contribution of each chain and each CDR to total BSA, (K) CDR3α-mediated interactions with PE, (L) CDR1α-mediated interactions with PE, and (M) CDR3β-mediated interactions with PE. Lymphocyte receptor residues are labeled in black, PE α-peptide residues are labeled in pink, and PE β-peptide residues are labeled in light pink. Hydrogen bond and salt bridge interactions are shown as black dashed lines. Contacting residues are shown as sticks. Not all contact residues are displayed. PEB, phycoerythrobilin.

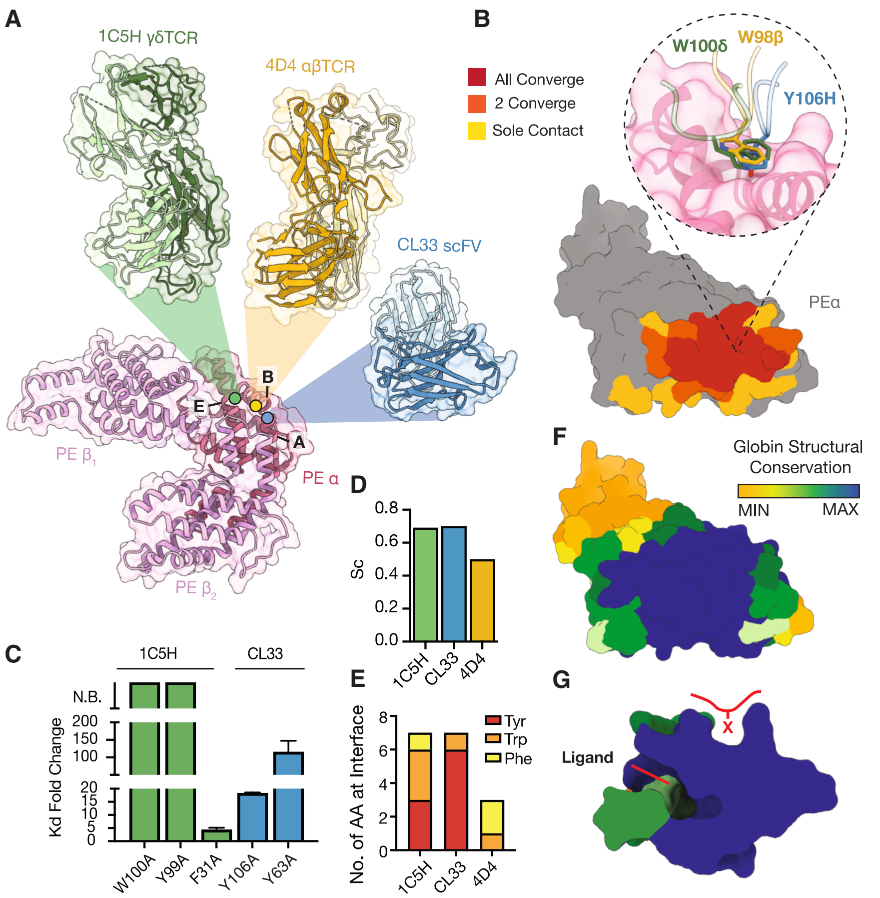

Figure 5. PE-reactive lymphocyte receptors converge on a single epitope

(A) Structural docking arrangement of all three lymphocyte receptors binding PE.

(B) Overlayed footprint of recognition by the three receptors on PE surface, residues contacted by one receptor are colored yellow, those contacted by two are colored orange, and residues contacted by all three receptors are colored red. Conserved aromatic used to probe hydrophobic pocket shown zoomed from conserved recognition zone.

(C) Alanine point mutational SPR of 1C5H γδTCR and CL33 scFv passaged over immobilized PE, depicted as fold change in K_D from wild type receptor measured in parallel. N.B, no binding. K_D measured from two independent expressions of analyte within one experiment. Error bars represent mean and SEM.

(D) Comparative analysis of shape complementarity (Sc) of each receptor bound PE surface, Sc calculated using CCP4 Software.

(E) Comparison of PE-contacting aromatic residues used at the interface of each receptor complex.

(F) PE α-chain structural conservation across the globin-like superfamily, using DALI alignment of the top 30 non-redundant homologous proteins.

(G) View of PE α-chain, depicting conserved ligand binding pocket that is recognized by the three different receptors. X depicts placement of the conserved lymphocyte receptor apical aromatic.

MHC-like molecule surface (Figure 6A), similar to antibody binding of MHC-like epitopes yet in stark contrast to the conserved αβTCR recognition modes (Figures 6B and 6C). The architecture of TCR Vδ (1/2/3) domains are broadly more similar to Ig variable heavy (VH) domains (root-mean-square deviation [RMSD] ~1.04/0.86//0.99 Å, respectively) than they are to Vα domains (RMSD ~1.25/1.11/1.19 Å, respectively). As noted previously, in Vδ3 domains, the C″ β-strand stacked alongside the C′ β-strand, as in the VH domain[43] (Figure 6D). This architecture is also mirrored in C″ β-strand of Vδ2 domains; however, in the Vδ1 domain, the C″ β-strand shifts to the opposing β-sheet of the IgV to stack alongside the D β-strand, as observed in Vα domains (Figure 6D). We next analyzed the conformational variance of the CDR loops within our structural sample set to reveal high dynamism of the CDR3δ, more so than the CDR3α but less dynamic than the CDR3H (Figure 6E).

We next utilized public structural databases of antibody/αβTCR structural complexes (SAbDab[44] and TCR3d[45]) as well as known antigen reactive γδTCR sequences across literature for our analyses of lymphocyte characteristics.[10–15,28,41] The TCR δ-chain is known to encode the most varied CDR3 loops of the V-domains alongside the Ig H chain,[46] the distended CDR3δ largely dominated 1C5H γδTCR recognition of PE. Indeed, this was evident in our sample set with the average CDR3δ length at 19.29 ± 0.32 and CDR3H at 16.01 ± 0.07 residues, significantly larger than Vα, Vβ, Vγ, and Ig variable light (VL) domains (13.38 ± 0.14, 14.15 ± 0.14, 12.99 ± 0.21, and 9.52 ± 0.02, respectively) (Figure 6F). Given the abundance of apical aromatic residues in PE recognition, we next plotted the relative abundance of aromatics within the CDR3 loops across the different V domains. This analysis revealed an enrichment of CDR3δ-encoded tryptophan, phenylalanine, and histidine residues, similar to the CDR3H (Figure 6G). A point where the CDR3δ differed was a minimal use of tyrosines compared to an enrichment within the CDR3H loop, a known virtue of antibodies,[47–49] while the CDR3γ loop was also enriched in tyrosine residues (Figure 6G). A trend also emerged for the lack of aromatics in both the CDR3α and CDR3β compared to antibody and γδTCR CDR3s (Figure 6G). Multiple sequence alignments revealed a common apical tryptophan flanked by glycines within the CDR3δ (Figure 6H), this trend was not observed in the CDR3α. The Vδ domain thus presents as a structural midpoint between Vα and VH domains, in which a distended and aromatically enriched CDR3 loop provides unique "antibody-like" binding properties to diverse structural epitopes.

The molecular drivers of PE reactivity are more commonly encoded for in γδTCRs and antibodies than αβTCRs, in congruence with the frequency of reactive populations noted for each lymphocyte receptor. Overall, we provide a structural comparison of how a common bacterial derived protein can be directly recognized by three different receptors of lymphoid origin in an antibody-like manner. Further, we provide a structural

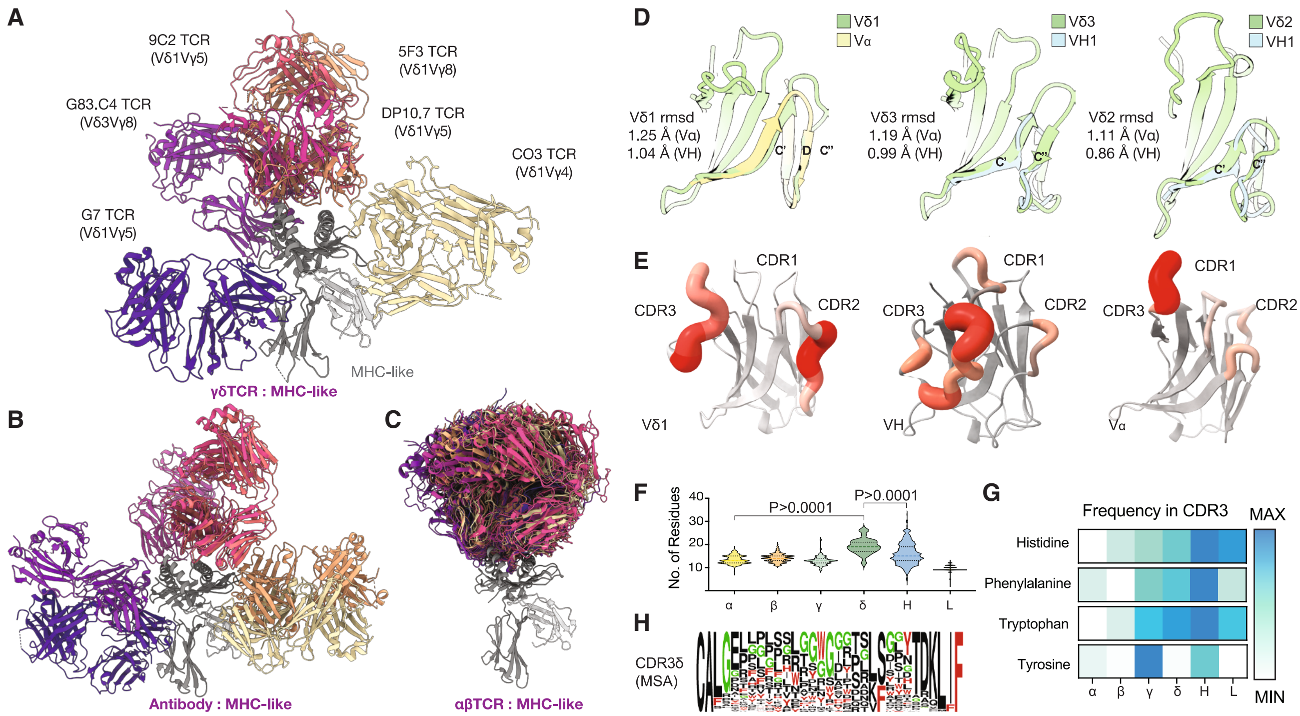

Figure 6. Intrinsic Properties of the γδTCR

(A) Overlay of six known γδTCR-MHC-like complexes, aligned to the MHC-like molecule, showing (represented by MR1).

(B) Overlay of seven known Fab-MHC-like complexes, aligned to the MHC-like molecule.

(C) Overlay of 150 known αβTCR-MHC-like complexes, aligned to the MHC-like molecule.

(D) Alignment of Vδ1-3 chains, with VH or Va. The Vδ2/3 C″ domains mirror VH while the Vδ1 C″ domain mirrors that of the Vα. RMSD depicted is an alignment of whole variable chains.

(E) Spatial distribution of CDRs adopted orientation in Vδ, VH, and Vα domains of MHC-like complexed lymphocyte receptors, displayed as putty, size, and color proportional to flexibility of orientation. Violin plot of number of amino acids comprising the CDR3 of each lymphocyte receptor variable chain.

(F) Violin plot of number of amino acids comprising the CDR3 of each lymphocyte receptor variable chain. Statistical significance was determined using one-way analysis of variance (ANOVA). *p* values represent significance from δ-chain length.

(G) Heatmap usage of each aromatic residue in the CDR3 of each lymphocyte receptor variable chain, colored from minimum 0% (MIN) to the highest percentage reported (MAX).

(H) Multiple sequence alignment of analyzed sequences of CDR3δ, aromatics and glycine shown in red and green, respectively.

(D–F) Analysis of structural data and sequences completed using structural databases of αβTCR, γδTCR, and antibody complexes (TCR3d 2.0 and SAbDab).[44,45] γδTCR sequence analysis utilized isolated ligand specific clones across literature due to lack of breadth in structural database.[10–15,27,43]

comparison of how these binding features are conserved by γδTCRs to recognizing different targets.

DISCUSSION

One of the lineage defining features of γδ T cells is the capacity for direct antigen engagement beyond the realms of MHC-restriction.[50] PE is a consistently identified antigen for B cells and γδ T cells, across species.[28,31,33] Through a broad range of biophysical assays, we confirmed the reactivity of two human Vδ1⁺ γδ T cells toward PE in a direct manner. Direct recognition of PE was immunostimulatory, triggering proximal γδTCR signaling and cellular activation. The 1C5H γδTCR-PE cryo-EM structure revealed antibody-like mechanisms to enable direct antigen binding. The 1C5H-PE structure revealed the ability of γδTCRs to bind non-MHC-like molecules in a CDR-dependent manner. The Vδ domain dominated the binding interface akin to the heavy chain in antibodies and distinct from αβTCRs balanced chain usage. The Vδ driven reactivity to PE was enabled by the unique characteristics of the CDR3δ, namely a distended CDR3δ that encoded an apical aromatic that dominated the TCR paratope. We determined the cryo-EM structures of three lymphocyte receptors (Ig, γδTCR, and αβTCR) in complex with a common antigen. These structures revealed convergent recognition of a PE α-chain pocket via the common use of a CDR3 aromatic.

As noted in antibody recognition, the PE-reactive γδTCR was enriched for apical aromatics within the γδTCR CDR3 loops.[40] Site-directed mutagenesis revealed the 1C5H γδTCR recognition of PE relied upon Y99 and W100 of the CDR3δ; the CL33 scFv was not reliant on similar aromatics while the role of aromatics in αβTCR recognition of PE is yet to be explored. Indeed, PE recognition by the 1C5H γδTCR was driven by W100δ of the CDR3δ. This resided within a "YWG" motif, which is present in half of the PE-reactive γδTCR clones identified (1C5H, BC14PE1, and HX9).[28,31] The others encoding a "WG" in either the δ chain (HX2 and HX3) or the γ chain (BC14PE3). This motif largely stems from the TRDD3*01 locus encoding "WGI" that is prefaced by an "AC" codon sequence, preferentially encoding a tyrosine, histidine, asparagine or aspartic acid to be transcribed before the inserted "WGI." This somatic recombination event, biased toward an apical "YWG" motif in the CDR3δ may be key to direct antigen engagement.

PE, although a bacterially encoded protein, is not pathogenic in nature and hence proves difficult to postulate as a disease-associated antigen. However, lymphocyte recognition of PE is both persistent and inducive of activation, and is therefore a useful model foreign antigen system in which to study immune receptor recognition. The potential for the multivalency of the PE antigen may induce or drive receptor clustering; this and the impact of Vγ5 TCR dimerization on signaling certainly merit future experimentation to discern their influence on cellular activation. Previous literature has stated most PE-reactive B cells bind to a single epitope; we uncover the molecular basis of this common epitope and confirm TCR reactivity to the same epitope. The immunological reason for lymphocyte reactivity to this globulin fold remains unknown. Further research may reveal the origins of this reactivity, whether it be an exploitation of apical hydrophobic elements of lymphocyte CDRs, or perhaps an instance of cross reactivity to structurally homologous proteins conserved from evolution events of pathogenic origin.

To understand the molecular basis of antibody-like recognition by the γδTCR, we analyzed MHC-like complexes.[12–15,41,42] We revealed that the Vδ domain structure and CDR length and composition resembles the VH domain. This included the C″ β-strand of the Vδ domain that adopts two conformations. In the Vδ2 and Vδ3, the β-strand conformation resembled an antibody, whereas the Vδ1 mimicked the Vα. Nonetheless, the Vδ domain IgVs are all most homologous to the IgVH. Further, the trend of Vδ-driven MHC-like reactivity of γδTCRs is in turn enabled by a CDR3δ that encodes apical aromatics.[51] These characteristics are shared, in whole, with the CDR3H of antibodies. Conversely, apical aromatics skew αβTCRs toward self-reactivity and rarely escape negative selection.[52] These emerging trends may not extend to Vδ2 TCRs that appear to mediate antigen recognition via dual CDR and non-CDR contacts.[53,54] Thus, the antibody-like reactivity of the γδTCR stems from an IgH-like Vδ domain tertiary structure that encodes a distended and aromatic CDR3δ.

This study has elucidated the structural framework of direct antigen binding by the γδTCR, alongside a scFv and αβTCR, which provided molecular insight into the reactivity. We depict conserved characteristics shared between γδTCRs and antibodies during antigen recognition. These mechanisms are central to PE recognition, but it is yet to be seen if these emergent trends continue for the many other γδ T cell antigens.

RESOURCE AVAILABILITY

Lead contact

Further information and requests for resources and reagents should be directed to and will be fulfilled by the lead contact, Jamie Rossjohn (jamie.rossjohn@monash.edu).

Materials availability

Reagents generated in this study are available from the lead contact.

Data and code availability

The link to cluster analysis algorithm used in this study is available at the GitHub repository link, https://github.com/PRNicovich/ClusDoC.[55] The atomic coordinates for all structures have been deposited at the Protein DataBank (https://www.ebi.ac.uk/pdbe/) under the following accession codes: PDB: 9O61 (PE), PDB: 9O62 (1C5H-PE), PDB: 9O60 (1C5H dimer), PDB: 9MGB (CL33-PE), and PDB: 9MKO (4D4-PE). Cryo-EM maps (B-factor-sharpened, -non-sharpened, half-maps, and appropriate masks) have been deposited at the Electron Microscopy DataBank (https://www.ebi.ac.uk/emdb/) under the following accession codes: EMD: 48248 (CL33-PE complex), EMD: 48332 (4D4-PE complex), EMD: 70157 (1C5H-PE composite map), EMD: 70155 (1C5H-PE TCR local refinement), EMD: 70139 (1C5H-PE consensus map), and EMD: 70156.[16] They are publicly available as of the date of publication. Accession codes are also listed in the key resources table. Any additional information required to reanalyze the data reported in this paper is available from the lead contact upon request.

ACKNOWLEDGMENTS

This work was supported by a Monash FMNHS Future Leaders Fellowship (to B.S.G.), National Health and Medical Research Council Investigator Awards (to J.R. (2008981), D.I.G. (2008913), and N.A.G (2027058)), Australian Research Council discovery grants (nos. DP200103462 and DP230102073 to B.S.G. and DP170104386 to D.I.G.), National Institutes of Health grants (R01 AI049313 and R01 AR048632 to D.B.M.), and an Australian Institute of Nuclear Science and Engineering Early Career Research Grant (M.T.R). We thank Dr. Ashish Sethi and staff at the Australian Synchrotron for assistance with data collection. S.D.G. would like to thank staff at Centre for Dynamic Imaging, WEHI for providing access to Single-Molecule Imaging microscope. We would also like to thank the staff at the Ramaciotti Centre for Cryo-Electron Microscopy and Monash Flowcore Facility for their assistance.

AUTHOR CONTRIBUTIONS

L.R. – collected, analysed data, wrote paper. H.V. – cryo-EM analyses. M.T.R., C.L.S. – biophysical analyses. S.D.G. – single molecule imaging analyses. N.A.G., C.F.A., I.V.R., D.B.M., D.I.G. – key reagents and revised manuscript. J.R. and B.S.G. – co-supervised project, co-wrote and revised paper. J.R. – project funding & lead contact.

DECLARATION OF INTERESTS

The authors declare no competing interests.

STAR★METHODS

Detailed methods are provided in the online version of this paper and include the following:

- KEY RESOURCES TABLE
- EXPERIMENTAL MODEL AND STUDY PARTICIPANT DETAILS
- METHOD DETAILS
  - Bacterial production of soluble proteins
  - Mammalian production of γδTCRs
  - Surface plasmon resonance
  - Complexation
  - SEC-SAXS
  - Production of stable TCR-transduced cell lines
  - Preparation of supported lipid bilayer (SLB)
  - Stimulating Jurkat T cells and BW58 thymoma cells on SLB
  - Immunostaining of Jurkat T cells and BW58 thymoma cells
  - Single-molecule imaging with direct stochastic optical reconstruction microscopy (*d*STORM)
  - Cluster analysis of single-molecule images
  - Statistical analyses
  - Plate bound activation assays
  - Negative stain electron microscopy
  - Cryo-EM sample preparation

- ○ 1C5H-PE titan krios collection
- ○ CL33-PE & 4D4-PE talos arctica collection
- ○ Cryo-EM data processing
- ○ Atomic building and refinement
- ○ Data analysis
- ● QUANTIFICATION AND STATISTICAL ANALYSIS

SUPPLEMENTAL INFORMATION

Supplemental information can be found online at https://doi.org/10.1016/j.str.2025.07.006.

Received: January 27, 2025
Revised: May 16, 2025
Accepted: July 4, 2025

REFERENCES

1. Godfrey, D.I., Uldrich, A.P., McCluskey, J., Rossjohn, J., and Moody, D.B. (2015). The burgeoning family of unconventional T cells. Nat. Immunol. *16*, 1114–1123. https://doi.org/10.1038/ni.3298.
2. Davey, M.S., Willcox, C.R., Baker, A.T., Hunter, S., and Willcox, B.E. (2018). Recasting Human Vdelta1 Lymphocytes in an Adaptive Role. Trends Immunol. *39*, 446–459. https://doi.org/10.1016/j.it.2018.03.003.
3. Silva-Santos, B., Serre, K., and Norell, H. (2015). gammadelta T cells in cancer. Nat. Rev. Immunol. *15*, 683–691. https://doi.org/10.1038/nri3904.
4. Halary, F., Pitard, V., Dlubek, D., Krzysiek, R., de la Salle, H., Merville, P., Dromer, C., Emilie, D., Moreau, J.F., and Déchanet-Merville, J. (2005). Shared reactivity of Vdelta2(neg) gammadelta T cells against cytomegalovirus-infected cells and tumor intestinal epithelial cells. J. Exp. Med. *201*, 1567–1578. https://doi.org/10.1084/jem.20041851.
5. Roy Chowdhury, R., Valainis, J.R., Dubey, M., von Boehmer, L., Sola, E., Wilhelmy, J., Guo, J., Kask, O., Ohanyan, M., Sun, M., et al. (2023). NK-like CD8(+) gammadelta T cells are expanded in persistent Mycobacterium tuberculosis infection. Sci. Immunol. *8*, eade3525. https://doi.org/10.1126/sciimmunol.ade3525.
6. Kotsias, F., Cebrian, I., and Alloatti, A. (2019). Antigen processing and presentation. Int. Rev. Cell Mol. Biol. *348*, 69–121. https://doi.org/10.1016/bs.ircmb.2019.07.005.
7. Rossjohn, J., Gras, S., Miles, J.J., Turner, S.J., Godfrey, D.I., and McCluskey, J. (2015). T cell antigen receptor recognition of antigen-presenting molecules. Annu. Rev. Immunol. *33*, 169–200. https://doi.org/10.1146/annurev-immunol-032414-112334.
8. Guo, J., Chowdhury, R.R., Mallajosyula, V., Xie, J., Dubey, M., Liu, Y., Li, J., Wei, Y.L., Palanski, B.A., Wang, C., et al. (2024). gammadelta T cell antigen receptor polyspecificity enables T cell responses to a broad range of immune challenges. Proc. Natl. Acad. Sci. USA *121*, e2315592121. https://doi.org/10.1073/pnas.2315592121.
9. Willcox, B.E., and Willcox, C.R. (2019). gammadelta TCR ligands: the quest to solve a 500-million-year-old mystery. Nat. Immunol. *20*, 121–128. https://doi.org/10.1038/s41590-018-0304-y.
10. Reijneveld, J.F., Ocampo, T.A., Shahine, A., Gully, B.S., Vantourout, P., Hayday, A.C., Rossjohn, J., Moody, D.B., and Van Rhijn, I. (2020). Human gammadelta T cells recognize CD1b by two distinct mechanisms. Proc. Natl. Acad. Sci. USA *117*, 22944–22952. https://doi.org/10.1073/pnas.2010545117.
11. Roy, S., Ly, D., Castro, C.D., Li, N.S., Hawk, A.J., Altman, J.D., Meredith, S.C., Piccirilli, J.A., Moody, D.B., and Adams, E.J. (2016). Molecular Analysis of Lipid-Reactive Vdelta1 gammadelta T Cells Identified by CD1c Tetramers. J. Immunol. *196*, 1933–1942. https://doi.org/10.4049/jimmunol.1502202.
12. Uldrich, A.P., Le Nours, J., Pellicci, D.G., Gherardin, N.A., McPherson, K. G., Lim, R.T., Patel, O., Beddoe, T., Gras, S., Rossjohn, J., and Godfrey, D. I. (2013). CD1d-lipid antigen recognition by the gammadelta TCR. Nat. Immunol. *14*, 1137–1145. https://doi.org/10.1038/ni.2713.
13. Luoma, A.M., Castro, C.D., Mayassi, T., Bembinster, L.A., Bai, L., Picard, D., Anderson, B., Scharf, L., Kung, J.E., Sibener, L.V., et al. (2013). Crystal structure of Vdelta1 T cell receptor in complex with CD1d-sulfatide shows MHC-like recognition of a self-lipid by human gammadelta T cells. Immunity *39*, 1032–1042. https://doi.org/10.1016/j.immuni.2013.11.001.
14. Le Nours, J., Gherardin, N.A., Ramarathinam, S.H., Awad, W., Wiede, F., Gully, B.S., Khandokar, Y., Praveena, T., Wubben, J.M., Sandow, J.J., et al. (2019). A class of gammadelta T cell receptors recognize the underside of the antigen-presenting molecule MR1. Science *366*, 1522–1527. https://doi.org/10.1126/science.aav3900.
15. Rice, M.T., von Borstel, A., Chevour, P., Awad, W., Howson, L.J., Littler, D. R., Gherardin, N.A., Le Nours, J., Giles, E.M., Berry, R., et al. (2021). Recognition of the antigen-presenting molecule MR1 by a Vdelta3(+) gammadelta T cell receptor. Proc. Natl. Acad. Sci. USA *118*, e2110288118. https://doi.org/10.1073/pnas.2110288118.
16. Rigau, M., Ostrouska, S., Fulford, T.S., Johnson, D.N., Woods, K., Ruan, Z., McWilliam, H.E.G., Hudson, C., Tutuka, C., Wheatley, A.K., et al. (2020). Butyrophilin 2A1 is essential for phosphoantigen reactivity by gammadelta T cells. Science *367*, eaay5516. https://doi.org/10.1126/science.aay5516.
17. Sandstrom, A., Peigne, C.M., Leger, A., Crooks, J.E., Konczak, F., Gesnel, M.C., Breathnach, R., Bonneville, M., Scotet, E., and Adams, E.J. (2014). The intracellular B30.2 domain of butyrophilin 3A1 binds phosphoantigens to mediate activation of human Vgamma9Vdelta2 T cells. Immunity *40*, 490–500. https://doi.org/10.1016/j.immuni.2014.03.003.
18. Willcox, C.R., Vantourout, P., Salim, M., Zlatareva, I., Melandri, D., Zanardo, L., George, R., Kjaer, S., Jeeves, M., Mohammed, F., et al. (2019). Butyrophilin-like 3 Directly Binds a Human Vgamma4(+) T Cell Receptor Using a Modality Distinct from Clonally-Restricted Antigen. Immunity *51*, 813–825.e4. https://doi.org/10.1016/j.immuni.2019.09.006.
19. Vavassori, S., Kumar, A., Wan, G.S., Ramanjaneyulu, G.S., Cavallari, M., El Daker, S., Beddoe, T., Theodossis, A., Williams, N.K., Gostick, E., et al. (2013). Butyrophilin 3A1 binds phosphorylated antigens and stimulates human gammadelta T cells. Nat. Immunol. *14*, 908–916. https://doi.org/10.1038/ni.2665.
20. Gu, S., Borowska, M.T., Boughter, C.T., and Adams, E.J. (2018). Butyrophilin3A proteins and Vgamma9Vdelta2 T cell activation. Semin. Cell Dev. Biol. *84*, 65–74. https://doi.org/10.1016/j.semcdb.2018.02.007.
21. Deseke, M., and Prinz, I. (2020). Ligand recognition by the gammadelta TCR and discrimination between homeostasis and stress conditions. Cell. Mol. Immunol. *17*, 914–924. https://doi.org/10.1038/s41423-020-0503-y.
22. Gully, B.S., Ferreira Fernandes, J., Gunasinghe, S.D., Vuong, M.T., Lui, Y., Rice, M.T., Rashleigh, L., Lay, C.S., Littler, D.R., Sharma, S., et al. (2024). Structure of a fully assembled gammadelta T cell antigen receptor. Nature *634*, 729–736. https://doi.org/10.1038/s41586-024-07920-0.
23. Xin, W., Huang, B., Chi, X., Liu, Y., Xu, M., Zhang, Y., Li, X., Su, Q., and Zhou, Q. (2024). Structures of human gammadelta T cell receptor-CD3 complex. Nature *630*, 222–229. https://doi.org/10.1038/s41586-024-07439-4.
24. Hoque, M., Grigg, J.B., Ramlall, T., Jones, J., McGoldrick, L.L., Lin, J.C., Olson, W.C., Smith, E., Franklin, M.C., Zhang, T., and Saotome, K. (2025). Structural characterization of two gammadelta TCR/CD3 complexes. Nat. Commun. *16*, 318. https://doi.org/10.1038/s41467-024-55467-5.
25. Harly, C., Joyce, S.P., Domblides, C., Bachelet, T., Pitard, V., Mannat, C., Pappalardo, A., Couzi, L., Netzer, S., Massara, L., et al. (2021). Human gammadelta T cell sensing of AMPK-dependent metabolic tumor reprogramming through TCR recognition of EphA2. Sci. Immunol. *6*, eaba9010. https://doi.org/10.1126/sciimmunol.aba9010.
26. Bruder, J., Siewert, K., Obermeier, B., Malotka, J., Scheinert, P., Kellermann, J., Ueda, T., Hohlfeld, R., and Dornmair, K. (2012). Target specificity of an autoreactive pathogenic human gammadelta-T cell receptor in myositis. J. Biol. Chem. *287*, 20986–20995. https://doi.org/10.1074/jbc.M112.356709.

27. Marlin, R., Pappalardo, A., Kaminski, H., Willcox, C.R., Pitard, V., Netzer, S., Khairallah, C., Lomenech, A.M., Harly, C., Bonneville, M., et al. (2017). Sensing of cell stress by human gammadelta TCR-dependent recognition of annexin A2. Proc. Natl. Acad. Sci. USA *114*, 3163–3168. https://doi.org/10.1073/pnas.1621052114.

28. Zeng, X., Wei, Y.L., Huang, J., Newell, E.W., Yu, H., Kidd, B.A., Kuhns, M. S., Waters, R.W., Davis, M.M., Weaver, C.T., and Chien, Y.H. (2012). gammadelta T cells recognize a microbial encoded B cell antigen to initiate a rapid antigen-specific interleukin-17 response. Immunity *37*, 524–534. https://doi.org/10.1016/j.immuni.2012.06.011.

29. Zeng, X., Meyer, C., Huang, J., Newell, E.W., Kidd, B.A., Wei, Y.L., and Chien, Y.H. (2014). Gamma delta T cells recognize haptens and mount a hapten-specific response. eLife *3*, e03609. https://doi.org/10.7554/eLife.03609.

30. Pape, K.A., Maul, R.W., Dileepan, T., Paustian, A.S., Gearhart, P.J., and Jenkins, M.K. (2018). Naive B Cells with High-Avidity Germline-Encoded Antigen Receptors Produce Persistent IgM(+) and Transient IgG(+) Memory B Cells. Immunity *48*, 1135–1143.e4. https://doi.org/10.1016/j.immuni.2018.04.019.

31. Almeida, C.F., Gully, B.S., Jones, C.M., Kedzierski, L., Gunasinghe, S.D., Rice, M.T., Berry, R., Gherardin, N.A., Nguyen, T.T., Mok, Y.F., et al. (2024). Direct recognition of an intact foreign protein by an alphabeta T cell receptor. Nat. Commun. *15*, 8816. https://doi.org/10.1038/s41467-024-51897-3.

32. Wu, C.J., Karttunen, J.T., Chin, D.H., Sen, D., and Gilbert, W. (1991). Murine memory B cells are multi-isotype expressors. Immunology *72*, 48–55.

33. Pape, K.A., Taylor, J.J., Maul, R.W., Gearhart, P.J., and Jenkins, M.K. (2011). Different B cell populations mediate early and late memory during an endogenous immune response. Science *331*, 1203–1207. https://doi.org/10.1126/science.1201730.

34. Eckle, S.B.G., Birkinshaw, R.W., Kostenko, L., Corbett, A.J., McWilliam, H. E.G., Reantragoon, R., Chen, Z., Gherardin, N.A., Beddoe, T., Liu, L., et al. (2014). A molecular basis underpinning the T cell receptor heterogeneity of mucosal-associated invariant T cells. J. Exp. Med. *211*, 1585–1600. https://doi.org/10.1084/jem.20140484.

35. Pellicci, D.G., Patel, O., Kjer-Nielsen, L., Pang, S.S., Sullivan, L.C., Kyparissoudis, K., Brooks, A.G., Reid, H.H., Gras, S., Lucet, I.S., et al. (2009). Differential recognition of CD1d-alpha-galactosyl ceramide by the V beta 8.2 and V beta 7 semi-invariant NKT T cell receptors. Immunity *31*, 47–59. https://doi.org/10.1016/j.immuni.2009.04.018.

36. Adams, E.J., Chien, Y.H., and Garcia, K.C. (2005). Structure of a gammadelta T cell receptor in complex with the nonclassical MHC T22. Science *308*, 227–231. https://doi.org/10.1126/science.1106885.

37. Hayakawa, K., Ishii, R., Yamasaki, K., Kishimoto, T., and Hardy, R.R. (1987). Isolation of high-affinity memory B cells: phycoerythrin as a probe for antigen-binding cells. Proc. Natl. Acad. Sci. USA *84*, 1379–1383. https://doi.org/10.1073/pnas.84.5.1379.

38. Tas, J.M.J., Mesin, L., Pasqual, G., Targ, S., Jacobsen, J.T., Mano, Y.M., Chen, C.S., Weill, J.C., Reynaud, C.A., Browne, E.P., et al. (2016). Visualizing antibody affinity maturation in germinal centers. Science *351*, 1048–1054. https://doi.org/10.1126/science.aad3439.

39. Jang, Y.J., Lecerf, J.M., and Stollar, B.D. (1996). Heavy chain dominance in the binding of DNA by a lupus mouse monoclonal autoantibody. Mol. Immunol. *33*, 197–210. https://doi.org/10.1016/0161-5890(95)00094-1.

40. Birtalan, S., Zhang, Y., Fellouse, F.A., Shao, L., Schaefer, G., and Sidhu, S. S. (2008). The intrinsic contributions of tyrosine, serine, glycine and arginine to the affinity and specificity of antibodies. J. Mol. Biol. *377*, 1518–1528. https://doi.org/10.1016/j.jmb.2008.01.093.

41. Wegrecki, M., Ocampo, T.A., Gunasinghe, S.D., von Borstel, A., Tin, S.Y., Reijneveld, J.F., Cao, T.P., Gully, B.S., Le Nours, J., Moody, D.B., et al. (2022). Atypical sideways recognition of CD1a by autoreactive gammadelta T cell receptors. Nat. Commun. *13*, 3872. https://doi.org/10.1038/s41467-022-31443-9.

42. Benveniste, P.M., Roy, S., Nakatsugawa, M., Chen, E.L.Y., Nguyen, L., Millar, D.G., Ohashi, P.S., Hirano, N., Adams, E.J., and Zúñiga-Pflücker, J.C. (2018). Generation and molecular recognition of melanoma-associated antigen-specific human gammadelta T cells. Sci. Immunol. *3*, eaav4036. https://doi.org/10.1126/sciimmunol.aav4036.

43. Li, H., Lebedeva, M.I., Llera, A.S., Fields, B.A., Brenner, M.B., and Mariuzza, R.A. (1998). Structure of the Vdelta domain of a human gammadelta T-cell antigen receptor. Nature *391*, 502–506. https://doi.org/10.1038/35172.

44. Dunbar, J., Krawczyk, K., Leem, J., Baker, T., Fuchs, A., Georges, G., Shi, J., and Deane, C.M. (2014). SAbDab: the structural antibody database. Nucleic Acids Res. *42*, D1140–D1146. https://doi.org/10.1093/nar/gkt1043.

45. Lin, V., Cheung, M., Gowthaman, R., Eisenberg, M., Baker, B.M., and Pierce, B.G. (2025). TCR3d 2.0: expanding the T cell receptor structure database with new structures, tools and interactions. Nucleic Acids Res. *53*, D604–D608. https://doi.org/10.1093/nar/gkae840.

46. Rock, E.P., Sibbald, P.R., Davis, M.M., and Chien, Y.H. (1994). CDR3 length in antigen-specific immune receptors. J. Exp. Med. *179*, 323–328. https://doi.org/10.1084/jem.179.1.323.

47. Peng, H.P., Lee, K.H., Jian, J.W., and Yang, A.S. (2014). Origins of specificity and affinity in antibody-protein interactions. Proc. Natl. Acad. Sci. USA *111*, E2656–E2665. https://doi.org/10.1073/pnas.1401131111.

48. Peng, H.P., Hsu, H.J., Yu, C.M., Hung, F.H., Tung, C.P., Huang, Y.C., Chen, C.Y., Tsai, P.H., and Yang, A.S. (2022). Antibody CDR amino acids underlying the functionality of antibody repertoires in recognizing diverse protein antigens. Sci. Rep. *12*, 12555. https://doi.org/10.1038/s41598-022-16841-9.

49. Zemlin, M., Klinger, M., Link, J., Zemlin, C., Bauer, K., Engler, J.A., Schroeder, H.W., Jr., and Kirkham, P.M. (2003). Expressed murine and human CDR-H3 intervals of equal length exhibit distinct repertoires that differ in their amino acid composition and predicted range of structures. J. Mol. Biol. *334*, 733–749. https://doi.org/10.1016/j.jmb.2003.10.007.

50. Vantourout, P., and Hayday, A. (2013). Six-of-the-best: unique contributions of gammadelta T cells to immunology. Nat. Rev. Immunol. *13*, 88–100. https://doi.org/10.1038/nri3384.

51. Sok, C.L., Rossjohn, J., and Gully, B.S. (2024). The Evolving Portrait of gammadelta TCR Recognition Determinants. J. Immunol. *213*, 543–552. https://doi.org/10.4049/jimmunol.2400114.

52. Stadinski, B.D., Shekhar, K., Gómez-Touriño, I., Jung, J., Sasaki, K., Sewell, A.K., Peakman, M., Chakraborty, A.K., and Huseby, E.S. (2016). Hydrophobic CDR3 residues promote the development of self-reactive T cells. Nat. Immunol. *17*, 946–955. https://doi.org/10.1038/ni.3491.

53. Fulford, T.S., Soliman, C., Castle, R.G., Rigau, M., Ruan, Z., Dolezal, O., Seneviratna, R., Brown, H.G., Hanssen, E., Hammet, A., et al. (2024). Vgamma9Vdelta2 T cells recognize butyrophilin 2A1 and 3A1 heteromers. Nat. Immunol. *25*, 1355–1366. https://doi.org/10.1038/s41590-024-01892-z.

54. Wang, H., Fang, Z., and Morita, C.T. (2010). Vgamma2Vdelta2 T Cell Receptor recognition of prenyl pyrophosphates is dependent on all CDRs. J. Immunol. *184*, 6209–6222. https://doi.org/10.4049/jimmunol.1000231.

55. Pageon, S.V., Nicovich, P.R., Mollazade, M., Tabarin, T., and Gaus, K. (2016). Clus-DoC: a combined cluster detection and colocalization analysis for single-molecule localization microscopy data. Mol. Biol. Cell *27*, 3627–3636. https://doi.org/10.1091/mbc.E16-07-0478.

56. Kjer-Nielsen, L., Borg, N.A., Pellicci, D.G., Beddoe, T., Kostenko, L., Clements, C.S., Williamson, N.A., Smyth, M.J., Besra, G.S., Reid, H.H., et al. (2006). A structural basis for selection and cross-species reactivity of the semi-invariant NKT cell receptor in CD1d/glycolipid recognition. J. Exp. Med. *203*, 661–673. https://doi.org/10.1084/jem.20051777.

57. Hopkins, J.B. (2024). BioXTAS RAW 2: new developments for a free open-source program for small-angle scattering data reduction and analysis. J. Appl. Crystallogr. *57*, 194–208. https://doi.org/10.1107/S1600576723011019.

58. Pageon, S.V., Tabarin, T., Yamamoto, Y., Ma, Y., Nicovich, P.R., Bridgeman, J.S., Cohnen, A., Benzing, C., Gao, Y., Crowther, M.D., et al. (2016). Functional role of T-cell receptor nanoclusters in signal initiation and antigen discrimination. Proc. Natl. Acad. Sci. USA *113*, E5454–E5463. https://doi.org/10.1073/pnas.1607436113.

59. Tang, G., Peng, L., Baldwin, P.R., Mann, D.S., Jiang, W., Rees, I., and Ludtke, S.J. (2007). EMAN2: an extensible image processing suite for electron microscopy. J. Struct. Biol. *157*, 38–46. https://doi.org/10.1016/j.jsb.2006.05.009.

60. Li, X., Mooney, P., Zheng, S., Booth, C.R., Braunfeld, M.B., Gubbens, S., Agard, D.A., and Cheng, Y. (2013). Electron counting and beam-induced motion correction enable near-atomic-resolution single-particle cryo-EM. Nat. Methods *10*, 584–590. https://doi.org/10.1038/nmeth.2472.

61. Kimanius, D., Forsberg, B.O., Scheres, S.H., and Lindahl, E. (2016). Accelerated cryo-EM structure determination with parallelisation using GPUs in RELION-2. eLife *5*, e18722. https://doi.org/10.7554/eLife.18722.

62. Punjani, A., Rubinstein, J.L., Fleet, D.J., and Brubaker, M.A. (2017). cryoSPARC: algorithms for rapid unsupervised cryo-EM structure determination. Nat. Methods *14*, 290–296. https://doi.org/10.1038/nmeth.4169.

63. Contreras-Martel, C., Martinez-Oyanedel, J., Bunster, M., Legrand, P., Piras, C., Vernede, X., and Fontecilla-Camps, J.C. (2001). Crystallization and 2.2 A resolution structure of R-phycoerythrin from Gracilaria chilensis: a case of perfect hemihedral twinning. Acta Crystallogr. D Biol. Crystallogr. *57*, 52–60. https://doi.org/10.1107/s0907444900015274.

64. Adams, P.D., Afonine, P.V., Bunkóczi, G., Chen, V.B., Davis, I.W., Echols, N., Headd, J.J., Hung, L.W., Kapral, G.J., Grosse-Kunstleve, R.W., et al. (2010). PHENIX: a comprehensive Python-based system for macromolecular structure solution. Acta Crystallogr. D Biol. Crystallogr. *66*, 213–221. https://doi.org/10.1107/S0907444909052925.

65. Emsley, P., and Cowtan, K. (2004). Coot: model-building tools for molecular graphics. Acta Crystallogr. D Biol. Crystallogr. *60*, 2126–2132. https://doi.org/10.1107/S0907444904019158.

66. Adams, P.D., Afonine, P.V., Bunkóczi, G., Chen, V.B., Echols, N., Headd, J.J., Hung, L.W., Jain, S., Kapral, G.J., Grosse Kunstleve, R.W., et al. (2011). The Phenix software for automated determination of macromolecular structures. Methods *55*, 94–106. https://doi.org/10.1016/j.ymeth.2011.07.005.

67. Meng, E.C., Goddard, T.D., Pettersen, E.F., Couch, G.S., Pearson, Z.J., Morris, J.H., and Ferrin, T.E. (2023). UCSF ChimeraX: Tools for structure building and analysis. Protein Sci. *32*, e4792. https://doi.org/10.1002/pro.4792.

STAR★METHODS

KEY RESOURCES TABLE

REAGENT or RESOURCE	SOURCE	IDENTIFIER
Antibodies		
anti-mouse CD3 (145-2C11)	eBioscience	Cat#14-0031-82; RRID: AB_467049
anti-mouse CD28 (37.51)	Invitrogen	Cat#13-0281-82; RRID: AB_467190
anti-human CD3ε (UCHT1)	BioLegend	Cat#300401; RRID: AB_314055
anti-mouse TCRβ (H57-597)	BioLegend	Cat#109207; RRID: AB_313430
anti-pCD3ζ-AF647	BD Biosciences	Cat#558402; RRID: AB_396815
anti-human CD3ε (OKT3)	eBioscience	Cat#16-0037-81; RRID: AB_468854
anti-human CD28 (CD28.2)	eBioscience	Cat#14-0289-82; RRID: AB_467194
anti-human CD3ε BUV-395 (OKT3)	BD Biosciences	Cat#563548; RRID: AB_2744387
anti-human CD69 APC (FN50)	BD Biosciences	Cat#555533; RRID: AB_398602
anti-Nur77 AF-647 (12.14)	BD Biosciences	Cat#566735; RRID: AB_2869837
anti-mouse CD3 BV711 (37.51)	BD Biosciences	Cat#563794; RRID: AB_2740409
anti-mouse CD69 APC (H12F3)	BD Biosciences	Cat#560689; RRID: AB_1727506
Bacterial and virus strains		
BL21 *Escherichia coli* (DE3)	New England Biolabs	Cat#C2527H
Chemicals, peptides, and recombinant proteins		
R-Phycoerythrin	Prozyme	Cat#PB31
Phycoerythrin-Streptavidin	Invitrogen	Cat#434301
Deposited data		
PE cryo-EM Reconstruction	This paper	EMD-70156
PE Model Coordinates	This paper	PDB-9O61
1C5H-PE cryo-EM Reconstruction (composite)	This paper	EMD-70157
1C5H-PE Model Coordinates	This paper	PDB-9O62
1C5H-PE consensus map	This paper	EMD-70139
1C5H dimer cryo-EM Reconstruction (local)	This paper	EMD-70155
1C5H dimer Model Coordinates	This paper	PDB-9O60
CL33-PE cryo-EM Reconstruction	This paper	EMD-48248
CL33-PE Model Coordinates	This paper	PDB-9MGB
4D4-PE cryo-EM Reconstruction	This paper	EMD-48332
4D4-PE Model Coordinates	This paper	PDB-9MKO
Experimental models: Cell lines		
Expi293F Cells	Gibco	Cat#A14527
BW5147.TCR $\alpha\beta^-$ thymoma cells	maintained in house> 10 years	N/A
Jurkat76 cells	maintained in house > 10 years	N/A
Software and algorithms		
MotionCor v2	Li et al.[60]	https://emcore.ucsf.edu/ucsf-software
RELION v2.0	Kimanius et al.[61]	https://relion.readthedocs.io/en/release-5.0/
cryoSPARC v4.0	Punjani et al.[62]	https://cryosparc.com
ChimeraX v1.8	Meng et al.[67]	https://www.cgl.ucsf.edu/chimerax/
Phenix v1.20.1	Adams et al.[64]	https://www.phenix-online.org/
COOT v0.9	Emsley et al.[65]	https://www2.mrc-lmb.cam.ac.uk/personal/pemsley/coot/
GraphPad Prism v10	Dotmatics	https://www.graphpad.com/features
EMAN2 v2.99	Tang et al.[59]	N/A

(*Continued on next page*)

Please cite this article in press as: Rashleigh et al., Antibody-like recognition of a γδ T cell receptor toward a foreign antigen, Structure (2025), https://doi.org/10.1016/j.str.2025.07.006

Continued		
REAGENT or RESOURCE	SOURCE	IDENTIFIER
BioXTAS RAW v2.1.4	Hopkins et al.[57]	https://bioxtas-raw.readthedocs.io/en/latest/
Cluster Analysis Algorithm v1	Pageon et al.[55]	https://github.com/PRNicovich/ClusDoC
FlowJo v10.10	BD	https://www.flowjo.com/

EXPERIMENTAL MODEL AND STUDY PARTICIPANT DETAILS

Soluble refolded proteins (CL33, 4D4, AF7, MR1-5-OP-RU) were produced utilising BL21 *Escherichia coli* (DE3) (New England Biolabs). Soluble mammalian produced proteins (1C5H, BC14PE1, BC14PE3) were expressed in Expi293F cells. Murine αβTCR clones (4D4 and 2C12) were retrovirally transduced in BW5147.TCR $\alpha\beta^{-}$ thymoma cells (termed BW58) and human γδTCR clones (1C5H or G83.C4) were transduced in Jurkat76 cells for cellular experiments.

METHOD DETAILS

Bacterial production of soluble proteins

CL33 scFv and CL33 scFv mutant cDNA constructs were ordered in pET30 vectors (Genscript) for inclusion body expression in BL21 *Escherichia coli* (DE3) (New England Biolabs). Purified inclusion bodies were resuspended (with their paired chains when appropriate) in 1 L of 3- 5 M Urea, 100 mM Tris-HCl pH 8.0, 2 mM Na-EDTA, 0.4 M L-arginine-HCl, 0.5 mM oxidized glutathione, 5 mM reduced glutathione and 0.2 mM PMSF then let to stir for 72 hours at 4°C. Following this, the refold suspension was extensively dialysed in 15 L of 10 mM Tris-HCl pH 8.0. Dialysis buffer was replaced following 3, 9 and 24 hours. Refolded soluble proteins were purified via anion exchange using DEAE resin (Sigma Aldrich). Samples were further purified via size-exclusion chromatography using a HiLoad 16/60 Superdex 200 pg column (GE Healthcare Life Sciences) followed by Anion Exchange Chromatography using a 1 mL HiTrapQ column (GE Healthcare Life Sciences). 4D4 αβTCR, AF7 αβTCR, CD1d-α-GalCer (KRS7000) and MR1-5-OP-RU were produced as previously described.[31,34,56]

Mammalian production of γδTCRs

1C5Hδ, 1C5Hγ, 1C5H mutations, BC14PE1δ, BC14PE1γ, BC14PE3δ and BC14PE3γ cDNA constructs were ordered in pcDNA3.1 vectors (Genscript) for Expi293F mammalian cell expression utilising TRGC1 and TRDC1 constant domains. Dulbecco's phosphate-buffered saline (Gibco) at a volume of 10% final culture volume was mixed with 0.5 μg/mL (culture volume) of corresponding γ and δ chain vectors. 4 μg/mL of linear polyethylenimine (Polysciences) was then added and the solution incubated at RT for 20 minutes. The final solution was then added to the Expi293F culture. The glucose concentration was adjusted to 33 mmol/L using D-Glucose (Sigma Aldrich). The culture was incubated for 24 hours before the addition of Minimum Essential Medium Non-Essential Amino Acids (MEM NEAA, Gibco, 100x) at a 2x concentration. After a further 48 hours of incubation, glucose concentration was checked and adjusted to 33 mmol/L again, 2 mM L-alanyl-L-glutamine was also added (Glutamax, Gibco). The culture was incubated for a further 48 hours before glucose adjustment to 33 mmol/L and the addition of 2x MEM NEAA. The harvested supernatant was extensively dialysed in 15 L of 10 mM Tris-HCl, 300 mM NaCl pH 8.0 with the buffer being replaced at 3, 9 and 24 hours. TCRs were purified *via* nickel affinity chromatography using Nickel-NTA resin (Qiagen) followed by size-exclusion chromatography using a HiLoad 16/60 Superdex 200 pg column. TCR samples were then left overnight at 4°C with an addition of 1 mM CaCl2 and 2 units of Thrombin (Sigma Aldrich) per 1 mg TCR followed by incubation at 37°C for 2 hours. Samples were finally purified via size-exclusion chromatography using a Superdex 200 Increase 10/300 column.

Surface plasmon resonance

Experiments were conducted using a CM5 Sensor Chip (Cytiva) in a Biacore T200 (Cytiva) or Biacore 3000 (Cytiva) at 25°C in 20 mM Hepes-HCl pH 7.4, 200 mM NaCl, 0.5% bovine serum albumin (Sigma Aldrich). 1000 response units of PE (Prozyme PB31) or MR1-5-OP-RU were immobilised to the chip via amine coupling. Graded concentrations of soluble AF7, 4D4, BC14PE1, 1C5H, BC14PE3 TCR or CL33 scFv were passed over test and control surfaces at 10 μl/min. GraphPad Prism 10 was used to generate graphical representations of sensorgrams and affinity curves as well as statistical analysis.

Complexation

Soluble T cell or B cell receptors were added at an 8:1 molar ratio to PE and left overnight at 4°C. The mixture was then purified via size-exclusion chromatography using a Superdex 200 Increase 10/300 column and assessed for complexation. Shifted peaks, indicative of complex formation, were pooled for structural experiments via SEC-SAXS or cryo-EM.

SEC-SAXS

In-line Size Exclusion Chromatography (HPLC) SAXs measurements were conducted at the SAXs/WAXs beamline of the Australian Synchrotron with continuous data collection on a 1 M Pilatus detector with a q range (Å1) of 0.006-0.420. Scattering data at maximal elution of the first UV peak was used for data processing. The radius of gyration,[45] maximum dimension (Dmax) and P(r) distribution plots of the samples were determined with the BioXTAS RAW software.[57] The automated Dmax determination by GNOM was used. Ab initio reconstructions were generated using DAMMIF, and ten independent reconstructions were superimposed and averaged using DAMAVER in the BioXTAS RAW software suite version.

Production of stable TCR-transduced cell lines

Murine αβTCR clones 4D4 and 2C12 were retrovirally transduced in BW5147.TCR $\alpha\beta^-$ thymoma cells (termed BW58) and human γδTCR clones 1C5H or G83.C4 were transduced in Jurkat76 cells as previously described.[14,31]

Preparation of supported lipid bilayer (SLB)

Glass coverslips (0.17 mm thickness) were cleaned sequentially with 1 M KOH and Milli-Q water, followed by immersion in 100% ethanol. The ethanol was allowed to evaporate in a fume hood, and the coverslips were then plasma-cleaned. After cleaning, the coverslips were attached to eight-well silicon chambers (ibidi, #80841). A 1 mg/ml liposome solution was extruded to form the SLB, following established protocols.[58] The liposome composition consisted of 96.5% DOPC (1,2-dioleoyl-sn-glycero-3- phosphocholine), 2% DGS-NTA(Ni) (1,2-dioleoyl-sn- glycero-3-[(N-(5-amino-1-carboxypentyl)iminodiacetic acid)succinyl] (nickel salt)), 1% Biotinyl-Cap-PE (1,2-dioleoyl-sn-glycero-3-phosphoethanolamine-N-(cap biotinyl) (sodium salt), and 0.5% PEG5000-PE (1,2-distearoyl-sn-glycero-3-phosphoethanolamine-N-[methoxy(poly-ethyleneglycol)-5000] (ammonium salt) (all purchased from Avanti Polar Lipids). The extruded liposomes were diluted (1:5) with Milli-Q water and 10 mM CaCl2, then incubated in the wells at room temperature for 30 minutes. After incubation, the wells were gently rinsed with PBS to remove unbound liposomes, while ensuring that approximately 200 μl of PBS remained in each well to minimize disruption of the SLB during washing steps. To assess the lateral mobility of the SLB, Fluorescence Recovery After Photobleaching (FRAP) was performed using fluorescent streptavidin (Invitrogen, #S11223).[58] After FRAP, excess Ca2+ was removed by adding 0.5 mM EDTA, followed by gentle rinsing with Milli-Q water. The functionalized NTA groups in the DGS-NTA(Ni) lipids were recharged by incubating the SLB with 1 mM NiCl2 for 15 minutes, after which excess Ni2+ was removed by repeated PBS washes.

Stimulating Jurkat T cells and BW58 thymoma cells on SLB

To further functionalize the SLB, 500 ng/ml of PE-streptavidin (BD Pharmingen, #554061) was coupled directly to the biotinylated lipids on the SLB. Following this, 500 ng/ml of either biotinylated human CD1d-α-GalCer or biotinylated antibodies of anti-mouse CD3 (Invitrogen, #13-0031-82, clone 145-2C11) with anti-mouse CD28 (Invitrogen, #13-0281-82, clone 37.51) or anti-human CD3 (Invitrogen, # 13-0037-82, clone OKT3) with anti-human CD28 (Invitrogen, 13-0289-82, clone CD28.2) were added. Prior to antibody coupling, 100 μg/ml of non-fluorescent streptavidin (Invitrogen, #434301) was used to bind the biotin groups on the SLB. For the unstimulated control condition, 200 ng/ml of His-tagged mouse ICAM-1 (Sino Biological, #50440-MO8H) or His-tagged human ICAM-1 (Sino Biological, #10346-H08H) was coupled directly to the NTA groups on the SLB. Once the SLB was functionalized with the appropriate ligands, it was rinsed thoroughly with PBS to remove any unbound proteins. Before adding Jurkat-76 T cells or BW58 cells expressing different TCRs (1C5H or G83.C4 in Jurkat-76 T cells and 4D4 or 2C12 in BW58 cells), the SLB was incubated in prewarmed RPMI culture medium (37°C) for 30 minutes. Cells were then introduced onto the SLB and allowed to activate for 5 minutes at 37°C. Cell fixation was achieved by treating the samples with 4% paraformaldehyde (vol/vol) in PBS for 15 minutes at room temperature. Excess fixative was removed by washing the samples thrice with PBS.

Immunostaining of Jurkat T cells and BW58 thymoma cells

Prior to immunostaining, cell lines were permeabilized with 0.1% (vol/vol) Triton X-100 (Sigma-Aldrich) for 15 minutes and subsequently rinsed thrice with PBS. To minimize non-specific binding, cells were blocked using a 5% bovine serum albumin solution in PBS. TCRs on cells were stained with a primary antibody targeting the human CD3ε or mouse TCRβ subunit, conjugated to Alexa Fluor 647 (BioLegend, #300416, Clone UCHT1 or BioLegend, #109218, clone H57-597 respectively). In a parallel experiment, another set of cells stimulated on the SLB was stained with primary antibodies specific to pCD3ζ, conjugated to Alexa Fluor 647 (BD Biosciences, #558402), to detect phosphorylation within the human or mouse CD3 complex. Both antibody staining processes were carried out for 1 hour at room temperature. After incubation, samples were thoroughly washed with PBS to remove any unbound antibodies. A post-fixation step followed, using 4% paraformaldehyde (vol/vol) in PBS for 15 minutes. Finally, prior to imaging, 0.1 μm TetraSpeck microspheres (Invitrogen, #T7279) were embedded into the SLB to serve as fiducial markers for alignment during imaging.

Single-molecule imaging with direct stochastic optical reconstruction microscopy (*d*STORM)

For *d*STORM imaging, a specialized imaging buffer consisting of TN buffer (50 mM Tris-HCl pH 8.0, 10 mM NaCl), an oxygen scavenging system (GLOX) [0.5 mg/ml glucose oxidase (Sigma-Aldrich, #G2133); 40 mg/ml catalase (Sigma-Aldrich, #C-100); and 10% w/v glucose], and 10 mM 2-aminoethanethiol (MEA; Sigma-Aldrich, #M6500) was prepared. Imaging was performed on a Nikon N-STORM 5.0 total internal reflection fluorescence (TIRF) microscope, equipped with a ×100/1.49 NA oil-immersion objective and lasers at 405, 473, 561, and 640 nm. Time series of 10,000 frames were captured for each sample at near-TIRF angle using 40% 640 nm and 5% 405 nm laser power, with an exposure time of 30 ms per frame. Before the acquisition, a brief photobleaching step (10-20 s using 90% 640 nm laser power) was performed to minimize fluorescence interference from phycoerythrin due to spectral bleed-through into the far-red channel. Fluorescence detection was carried out using a Hamamatsu Orca-Flash 4.0 V3 sCMOS

Please cite this article in press as: Rashleigh et al., Antibody-like recognition of a γδ T cell receptor toward a foreign antigen, Structure (2025), https://doi.org/10.1016/j.str.2025.07.006

camera. Image processing, including fiducial marker-based drift correction and the generation of x-y particle coordinates for localizations, was conducted using NIS-Elements AR software (version 5.2).

Cluster analysis of single-molecule images

To quantify cluster parameters in single-molecule images, we applied density-based spatial clustering of applications with noise (DBSCAN), using an algorithm implemented in MATLAB as previously described.[55] This approach allowed us to identify and quantify individual receptor clusters by defining a minimum number of neighbours (set to 3) and the radius within which these neighbours are located (r = 20 nm). From this analysis, we determined key cluster parameters such as the total number of detectable receptor clusters, their total area of occupancy, and the localizations within each cluster.

Statistical analyses

When comparing multiple groups, statistical analysis and P-values were calculated using one-way analysis of variance followed by Tukey's multiple comparisons test in GraphPad Prism software (v.10.2.0).

Plate bound activation assays

S-PE (BD Biosciences), human or murine anti-CD3 monoclonal (human OKT3, murine 145-2C11) and anti-CD28 (human CD28.2 and murine 37.51) monoclonal antibodies (Thermo Fisher), human MR1-5-OP-RU or murine CD1d-α-GalCer (KRN7000) in PBS were added to a 96 well flat bottom plate and titrated via serial dilution to displayed concentrations. Plates were spun at 1000g for 5 minutes before incubation at 37°C for 2 hours. Plates were then washed twice with PBS to remove unbound proteins. 50K cells were then dispensed and cultured for 2 (Nur77 Assay) or 16 hours (CD69/CD3 Assay) at 37°C. Cultures were then transferred to a 96 round bottom well plate for antibody staining. Cells were stained with Zombie Aqua live/dead stain (1:500 PBS) and left in the dark at RT for 10 minutes. Human Jurkat.76 cells were stained with anti-human CD3 (OKT3, BUV-395 BD Biosciences) and anti-human CD69 (FN50, Allophycocyanin (APC), BD Biosciences) or anti Nur77 (12.14, AF-647, BD Biosciences). Murine BW58 cells were stained with anti-murine CD3 (37.51, BV711) and anti-murine CD69 (H12F3, APC, BD Biosciences) or anti Nur77 (12.14, AF-647, BD Biosciences). CD69 and CD3 MFIs were assessed on a BD Fortessa. Data was analysed with FlowJo v10.10.

Negative stain electron microscopy

10 μl of purified CL33-PE complex particles at 0.1 mg/mL were hand blotted on Carbon support film grids (Pro SciTec) rendered hydrophilic by glow-discharging. After settling for three minutes samples were wicked with filter paper. This was followed by three rounds of Uranyl Acetate (2%) staining for 30 seconds before wicking and lastly air dried. Samples were imaged at a nominal 80,000x magnification using a JEOL 1400Plus transition electron microscope. Operating at a voltage of 120 kV, micrographs were recorded as a 2048 × 2048 pixel image at a pixel size of 2.25 Å. Data was processed through EMAN2 software through automatic particle picking and contrast transfer function (CTF) processing.[59] Reference free class averages were generated, and 'bad' particles manually removed. Good class-averages were used for initial model generation which was further refined through EMAN2 3D refinement.

Cryo-EM sample preparation

Cryo-EM grids of freshly purified receptor-PE complex were prepared by applying 3 μL at 1-3 mg/mL to UltrAuFoil® R1.2/1.3, Gold Mesh 300 grids (Quantifoil) and vitrified using a Vitribot Mark IV (Thermo Fisher Scientific), maintained at 4°C with 100% relative humidity.

1C5H-PE titan krios collection

For the 1C5H-PE complex data was collected on a Titan Krios G1 (Thermo Scientific) equipped with a Quantum energy filter (Gatan) and Summit K3 detector (Gatan). Operated at 300 kV with a 50 μM C2 aperture. A nominal magnification of x150,000 was used in counting mode which corresponded to a pixel size of 0.82 Å. 60 s exposure of 1 electron/pixel/s through a defocus range of -0.4 and -2.0 μM yielded a total dose of 60 electrons per Å2.

CL33-PE & 4D4-PE talos arctica collection

Frozen grids of CL33-PE or 4D4-PE complex were transferred to a Talos Arctica transmission electron microscope (FEI), operating at 200 kV with a 50 μM C2 aperture. Equipped with a bottom mounted Falcon 3 electron detector. A nominal magnification of x150,000 was used in counting mode which corresponded to a pixel size of 0.94 Å. 50 s exposure of 1 electron/pixel/s through a defocus range of -0.8 and -2.0 μM yielded a total dose of 50 electrons per Å2.

Cryo-EM data processing

Upon the collection of data, captured movies were aligned spatially. They were then corrected for beam-induced motion of particles during capture. For the 1C5H-PE sample, dose weighting and correction was conducted within MotionCor2.[60] CTF provides noise in projections of the object and is corrected for using Gctf software. Particles were picked using Gautomatch software (Khai Zhang). 2D classification occurred using RELION 2.0.[61] For the CL33-PE and 4D4-PE sample, motion correction was performed using Patch Motion, CTF correction was performed using Patch CTF and particles were picked using Blob picker of cryoSPARC v4.0. For all samples, 2D classification, 3D classification, heterogeneous refinement and homogeneous refinement were conducted using CryoSparc v4.0.[62]

Atomic building and refinement

Upon the final reconstructed cryo-EM map of 4D4-PE, the previous crystal structure of the complex was modelled into the map. Upon the final reconstructed cryo-EM map of 1C5H-PE, the crystal structure of a reference TCR 9C2 (4LFH.pdb[12]) and PE (1EYX.pdb[63]) were placed and modelled into the cryo- EM map. Upon the final reconstructed cryo-EM map of CL33-PE, previously refined PE and reference scFv structure (5YD3.pdb). Iterative model building and refinement using Phenix[64] was followed by manual rebuilding via COOT to determine the final model.[65,66] Structural graphics were prepared using ChimeraX.[67]

Data analysis

CDR sequences from known structures of TCR-ligand interactions were taken from the T cell receptor structural repertoire database, TCR3d.[45] CDR sequences from known antibody-ligand interactions were taken from the antibody structural database, SAbDab.[44] CDR sequences of ligand reactive γδTCRs were taken from previous publications.[10–15,28,41] Data was analysed using Microsoft Excel and GraphPad Prism10.

QUANTIFICATION AND STATISTICAL ANALYSIS

Cryo-EM data collection and refinement statistics are summarized in Table 1. GraphPad Prism software (v.10.2.0) was utilised for statistical analysis of data (details can be found in figure legends as well as method details).